
PREDICTIVE CODING APPROXIMATES BACKPROP ALONG ARBITRARY COMPUTATION GRAPHS

Beren Millidge

School of Informatics
University of Edinburgh
beren@millidge.name

Alexander Tschantz

Sackler Centre for Consciousness Science
School of Engineering and Informatics
University of Sussex
tschantz.alec@gmail.com

Christopher L Buckley

Evolutionary and Adaptive Systems Research Group
School of Engineering and Informatics
University of Sussex
C.L.Buckley@sussex.ac.uk

January 24, 2022

ABSTRACT

Backpropagation of error (backprop) is a powerful algorithm for training machine learning architectures through end-to-end differentiation. However, backprop is often criticised for lacking biological plausibility. Recently, it has been shown that backprop in multilayer-perceptrons (MLPs) can be approximated using predictive coding, a biologically-plausible process theory of cortical computation which relies only on local and Hebbian updates. The power of backprop, however, lies not in its instantiation in MLPs, but rather in the concept of automatic differentiation which allows for the optimisation of any differentiable program expressed as a computation graph. Here, we demonstrate that predictive coding converges asymptotically (and in practice rapidly) to exact backprop gradients on arbitrary computation graphs using only local learning rules. We apply this result to develop a straightforward strategy to translate core machine learning architectures into their predictive coding equivalents. We construct predictive coding CNNs, RNNs, and the more complex LSTMs, which include a non-layer-like branching internal graph structure and multiplicative interactions. Our models perform equivalently to backprop on challenging machine learning benchmarks, while utilising only local and (mostly) Hebbian plasticity. Our method raises the potential that standard machine learning algorithms could in principle be directly implemented in neural circuitry, and may also contribute to the development of completely distributed neuromorphic architectures.

1 Introduction

Deep learning has seen stunning successes in the last decade in computer vision (Krizhevsky, Sutskever, & Hinton, 2012; Szegedy et al., 2015), natural language processing and translation (Kaplan et al., 2020; Radford et al., 2019;

Vaswani et al., 2017), and computer game playing (Mnih et al., 2015; Schrittwieser et al., 2019; Silver et al., 2017; Vinyals et al., 2019). While there is a great variety of architectures and models, they are all underwritten by the core algorithm of automatic differentiation. The key insight is that it suffices to define a forward model which maps inputs to predictions according to some parameters. Then, using the chain rule of calculus, it is possible, as long as every operation of the forward model is differentiable, to differentiate back through the computation graph of the model so as to compute the sensitivity of every parameter in the model to the error at the output, and thus adjust every single parameter to best minimize the total loss. Early models were typically artificial neural networks where the computation graph is simply a composition of matrix multiplications and elementwise nonlinearities, and for which the implementation of automatic differentiation has become known as ‘backpropagation’ (or ‘backprop’). However, automatic differentiation allows for much more complicated graphs to be differentiated through, up to, and including, arbitrary programs (Baydin, Pearlmutter, Radul, & Siskind, 2017; Griewank et al., 1989; Innes et al., 2019; Paszke et al., 2017; Revels, Lubin, & Papamarkou, 2016). In recent years this has enabled the differentiation through differential equation solvers (T. Q. Chen, Rubanova, Bettencourt, & Duvenaud, 2018; Rackauckas et al., 2019; Tzen & Raginsky, 2019), physics engines (Degrave, Hermans, Dambre, & Wyffels, 2019; Heiden, Millard, & Sukhatme, 2019), raytracers (Pal, 2019), and planning algorithms (Amos & Yarats, 2019; Okada, Rigazio, & Aoshima, 2017). These advances allow the construction of models which intrinsically embody complex processes and encode significantly more prior knowledge and structure about a given problem domain than previously possible.

Modern deep learning has also been closely intertwined with neuroscience, with a succession of insights flowing both ways (Hassabis, Kumaran, Summerfield, & Botvinick, 2017; Hawkins & Blakeslee, 2007; Richards et al., 2019). Indeed, the backpropagation algorithm arose as a technique for training multi-layer perceptrons - simple hierarchical models of neurons inspired by the brain (Werbos, 1982). Despite this origin, and its empirical successes, a consensus has emerged that the brain cannot directly implement backprop, since to do so would require biologically implausible connection rules (Crick, 1989). There are two principal problems. The first is that backprop in the brain appears to require non-local information (since the activity of any specific neuron affects all subsequent neurons down to the final output neuron). It is difficult to see how this information could be transmitted ‘backwards’ throughout the brain with the required fidelity and without precise connectivity constraints. This is the credit-assignment problem. The second (smaller) problem is that backprop through MLP style networks requires identical forward and backwards weights, an additional problem called the ‘weight transport problem’. In recent years, however, a succession of models have been introduced which claim to implement backprop in MLP-style models using only biologically plausible connectivity schemes, and even Hebbian only learning rules (Bengio & Fischer, 2015; Bengio, Mesnard, Fischer, Zhang, & Wu, 2017; Guerguiev, Lillicrap, & Richards, 2017; Liao, Leibo, & Poggio, 2016; Ororbia, Mali, Giles, & Kifer, 2020; Sacramento, Costa, Bengio, & Senn, 2018; Whittington & Bogacz, 2019). Of particular significance is Whittington and Bogacz (2017) who show that predictive coding networks – a type of biologically plausible networks which can learn through a hierarchical process of prediction error minimization – are mathematically equivalent to backprop in MLP models. In this paper we extend this work, showing that predictive coding can not only approximate backprop in MLPs, but can approximate automatic differentiation along arbitrary computation graphs. This means that in theory there exist biologically plausible algorithms for differentiating through arbitrary programs, utilizing only local connectivity. Moreover, in a class of models which we call parameter-linear, which includes many current machine learning models, the required update rules are Hebbian, raising the possibility that a wide range of current machine learning architectures may be faithfully implemented in the brain, or in neuromorphic hardware.

In this paper we provide two main contributions. (i) We show that predictive coding converges to automatic differentiation across arbitrary computation graphs. (ii) We showcase this result by implementing three core machine learning architectures (CNNs, RNNs, and LSTMs) in a predictive coding framework which utilises only local learning rules and mostly Hebbian plasticity.

2 Predictive Coding Networks

Predictive coding is an influential theory of cortical function in theoretical and computational neuroscience. Central to the theory is the idea that the core function of the brain is to minimize prediction errors between what is expected to happen and what actually happens. On this view, the brain is composed of multiple hierarchical layers constantly trying to predict the activity of the layers below it. Unpredicted activity is registered as prediction-error which is then transmitted upwards for a higher layer to deal with. Over time, synaptic connections are adjusted so that the system as a whole improves at minimizing prediction error. Predictive coding possesses a wealth of empirical support (Bogacz, 2017; Friston, 2003, 2005; Whittington & Bogacz, 2019) and offers a single mechanism that accounts for diverse perceptual phenomena such as repetition-suppression (Auksztulewicz & Friston, 2016), end-stopping (Rao & Ballard, 1999), bistable perception (Hohwy, Roepstorff, & Friston, 2008; Weilnhammer, Stuke, Hesselmann, Sterzer, & Schmack, 2017) and illusory motions (Lotter, Kreiman, & Cox, 2016; Watanabe, Kitaoka, Sakamoto, Yasugi, & Tanaka, 2018), and even attentional modulation of neural activity (Feldman & Friston, 2010; Kanai, Komura, Shipp, & Friston, 2015). Moreover, the central role of top-down predictions is consistent with the ubiquity and importance of top-down diffuse connections between cortical areas. Predictive coding is consistent with many known aspects of neurophysiology, and has been translated into biologically plausible process theories which specify potential cortical microcircuits which could implement the algorithm. (Bastos et al., 2012; Kanai et al., 2015; Shipp, 2016; Spratling, 2008).

Mathematically, predictive coding corresponds to a variational inference algorithm under a hierarchical Gaussian generative model $p(y_0 \dots y_N) = p(y_0) \prod_{i=1}^N p(y_i|y_{i-1}) = \mathcal{N}(y_0; \bar{y}_0, \Sigma_0) \prod_{i=1}^N \mathcal{N}(y_i; f(y_{i-1}; \theta), \Sigma_i)$ (Buckley, Kim, McGregor, & Seth, 2017; Friston, 2005, 2008). In MLP models each y_i corresponds to a layer of the network. In an arbitrary computation graph, each y_i is the value of a vertex in the graph. Supposing we are given an input y_0 and a target y_N and we wish to infer the posterior distribution over all other variables. We approximate this intractable posterior through variational inference, by defining a variational distribution $Q(y; v, \sigma)$ ¹ and minimizing the variational free energy $\mathcal{F} = KL[Q(y_{1:N-1}; v_{1:N-1}, \sigma_{1:-1})||p(y_{1:N-1}, y_0, y_N)]$, an upper bound on the divergence between true and approximate posterior.

$$\begin{aligned} KL[Q(y_{1:N-1}; v_{1:N-1}, \sigma_{1:N-1})||p(y_{1:N-1}|y_0, y_N)] &= KL[Q(y_{1:N-1}; v_{1:N-1}, \sigma_{1:N-1})||p(y_{1:N-1}, y_0, y_N)] + \ln p(y_0, y_N) \\ &\leq -\mathcal{F} \end{aligned}$$

With a Gaussian form for the posterior and under the Laplace approximation, the form of the free-energy can be simplified considerably to a sum of prediction errors (see Appendix F). $-\mathcal{F} \approx \ln p(v_{1:N}, \Sigma_{1:N}) \approx \sum_{i=1}^N \epsilon_i^T \Sigma^{-1} \epsilon_i$ where $\epsilon_i = (y_i - f(y_{i-1}; \theta))$. For the rest of the paper we set all precisions (inverse variances) Σ^{-1} to the identity and henceforth ignore them². Biologically plausible and Hebbian learning rules for the variational parameters v and the parameters of the generative model θ (or activations and weights in machine learning terminology) can be derived as gradient descents on \mathcal{F} such that $\frac{dv_i}{dt} = -\frac{dF}{dv_i}$ and $\frac{d\theta_i}{dt} = -\frac{dF}{d\theta_i}$.

3 Related Work

A number of recent works have tried to provide biologically plausible approximations to backprop. The requirement of symmetry between the forwards and backwards weights has been questioned by Lillicrap, Cownden, Tweed, and Akerman (2016) who show that random fixed feedback weights suffice for effective learning. Recent additional work has shown that learning the backwards weights also helps (Akrout, Wilson, Humphreys, Lillicrap, & Tweed, 2019; Amit, 2019).

¹We use σ to distinguish the variational variance from the generative variance Σ . The variational variance σ is not necessarily scalar.

²This is equivalent to the assumption in backprop that all data is equally variable, and thus equally important.

A number of schemes have also been proposed to approximate backprop in a more biologically plausible manner, typically with local learning rules and/or Hebbian connectivity. These include target-prop (Lee, Zhang, Fischer, & Bengio, 2015) which approximate the backward gradients with trained inverse functions, but which fails to asymptotically compute the exact backprop gradients, and contrastive Hebbian (Scellier & Bengio, 2017; Scellier, Goyal, Binas, Mesnard, & Bengio, 2018; Seung, 2003) approaches which do exactly approximate backprop, but which require two separate learning phases and the storing of information across successive phases. There are also dendritic error theories (Guerguiev et al., 2017; Sacramento et al., 2018) which are computationally equivalent to predictive coding (Lillicrap, Santoro, Marris, Akerman, & Hinton, 2020; Whittington & Bogacz, 2019). Whittington and Bogacz (2017) showed that predictive coding can approximate backprop in MLP models, and demonstrated comparable performance on MNIST. We advance upon this work by extending the proof to arbitrary computation graphs, enabling the design of predictive coding variants of a range of standard machine learning architectures, which we show perform comparably to backprop on considerably more difficult tasks than MNIST. Our algorithm evinces asymptotic (and in practice rapid) convergence to the exact backprop gradients, does not require separate learning phases, and utilises only local information and largely Hebbian plasticity.

4 Predictive Coding on Computation Graphs

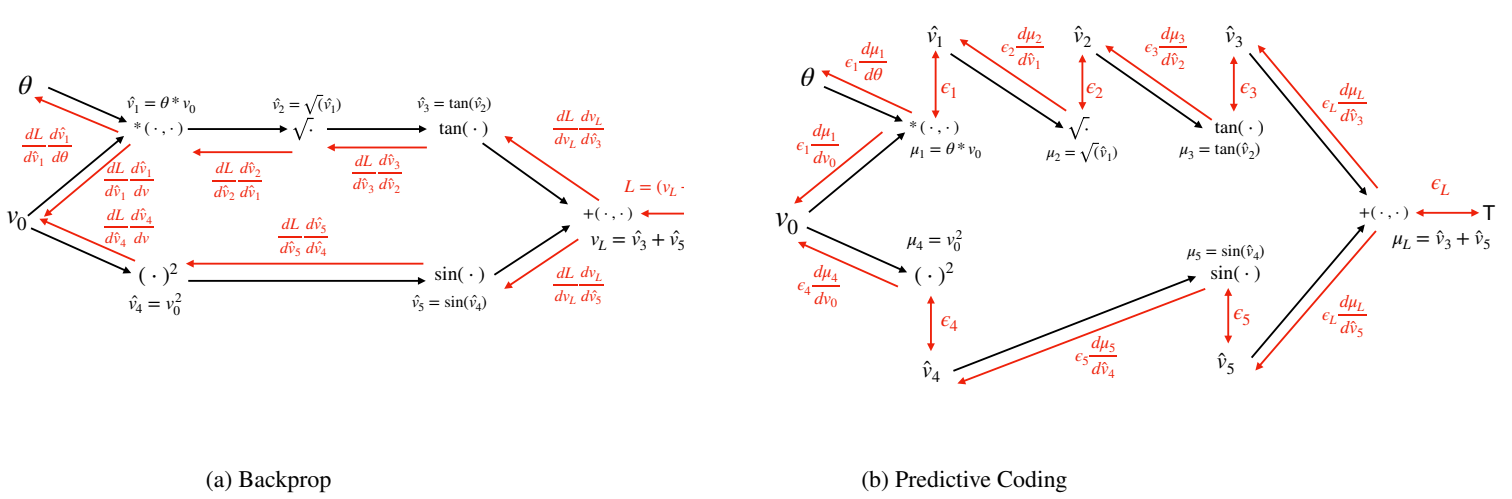


Figure 1: Information flow for backprop vs predictive coding on the arbitrary computation graph representing the test function $v_L = \tan(\sqrt{\theta}v_0) + \sin(v_0^2)$ (see Section 5.1). Backprop explicitly sends gradients backwards through the computation graph. Predictive coding augments each vertex of the graph with an error unit, and propagates these errors backwards, multiplied by the backwards derivatives. At equilibrium, $\epsilon_i^* = \frac{dL}{dv_{i+1}}$ and $\frac{d\mu_{i+1}^*}{dv_i^*} = \frac{dv_{i+1}^*}{dv_i^*}$ so the information passed back is the same in both algorithms.

A computation graph $\mathcal{G} = \{\mathbb{E}, \mathbb{V}\}$ is a directed acyclic graph (DAG) which can represent the computational flow of essentially any program or computable function as a composition of elementary functions. Each edge $e_i \in \mathbb{E}$ of the graph corresponds to an intermediate step – the application of an elementary function – while each vertex $v_i \in \mathbb{V}$ is an intermediate variable computed by applying the functions of the edges to the values of their originating vertices (each v_i can be a scalar, vector, or arbitrary tensor depending on the graph in question). Effectively, computation flows ‘forward’ from parent nodes to all their children until the leaf nodes give the final output of the program as a whole (see Figure 1 for an example). If a target T and a loss function $L = g(T, v_{out})$ are provided so that the goodness of the output can be evaluated, and every edge function is differentiable, automatic differentiation can be performed on the computation graph to obtain the derivative of every vertex v_i , and any parameters θ of any edge-function with

respect to the total loss L . These derivatives are computed by first computing the derivative at the output, and then recursively computing the derivatives of the parents of each node with respect to the output loss through the use of the chain rule $\frac{dL}{dv_i} = \sum_{j \in \text{Chi}(v_i)} \frac{dL}{dv_j} \frac{dv_j}{dv_i}$ where $\text{Chi}(v_i)$ is the set of children of the node v_i . Supposing that the child v_j depends on the parent v_i through some edge-function f with some parameters θ_i such that $v_j = f(v_i; \theta_i)$, the derivative of these parameters with respect to the loss function L can be computed as $\frac{dL}{d\theta_i} = \frac{dL}{dv_j} \frac{dv_j}{d\theta_i}$. By correctly computing the derivatives of any vertex or parameter within a graph with respect to the output, automatic differentiation (or backprop) exactly solves the credit assignment problem within complex computation graphs. Here we show that predictive coding can approximate correct backpropagated derivatives, down to numerical precision, on arbitrary computation graphs, using only local learning rules and without the need for separate forward and backward phases.

Predictive coding augments the computation graph with additional error units $\epsilon_i \in \mathcal{E}$, each associated with a particular vertex v_i . Moreover, unlike in backprop, the vertices v_i are considered random variables and their parents merely provide a prediction μ_i of the value of the vertex $\mu_i = f(\text{Par}(v_i))$ (where $\text{Par}(v_i)$ denotes the parents of v_i). The error unit measures the error of this prediction $\epsilon_i = v_i - \mu_i$. Given a fixed input v_0 and target T , we can cast finding the optimal values of the v_i 's as an inference problem which we can solve through variational inference using predictive coding. Recall from Section 2 that we can prescribe the dynamics of the vertices as a gradient descent on the variational free-energy $\mathcal{F} \propto \sum_i \epsilon_i^T \epsilon_i$.

$$\frac{dv_i}{dt} = -\frac{d\mathcal{F}}{dv_i} = \epsilon_i - \sum_{j \in \text{Chi}(v_i)} \epsilon_j \frac{d\mu_j}{dv_i} \quad (1)$$

The key fact, which we show below, is that at the equilibrium of the dynamics, the error units exactly encode the numerical gradient $\frac{dL}{dv_i}$. First, it is straightforward (a full derivation of the update rule and fixed point equations is presented in Appendix F) to solve for the fixed points of the error units ϵ_i^* and vertices v_i^*

$$\epsilon_i^* = \sum_{j \in \text{Chi}(v_i)} \epsilon_j^* \frac{d\mu_j}{dv_j} \Bigg|_{\mu_j^*, v_j^*} \quad \text{and} \quad v_i^* = \mu_i^* - \sum_{j \in \text{Chi}(v_i)} \epsilon_j^* \frac{d\mu_j}{dv_j} \Bigg|_{\mu_j^*, v_j^*} \quad (2)$$

To indicate that the derivatives of the predictions have to be taken at the equilibrium, we denote $\frac{d\mu_i}{dv_i} \Big|_{\mu_i^*, v_i^*} =: \frac{d\mu_i^*}{dv_i^*}$.

Next we show that at equilibrium the prediction errors correspond precisely to the backpropagated gradients, and the predictive coding weight update rules correspond directly to the backprop weight updates.

We first consider the terminal vertex of the graph and then recurse.³ The value of the terminal vertex is fixed to the target label $v_L = T$. We assume the mean-squared-error loss function $L = \frac{1}{2} \sum (T - \mu_L)^2$. Consider then the prediction error at the penultimate layer $\epsilon_{L-1} \in \text{Par}(v_L)$. At equilibrium, by Equation 2, we have:

$$\begin{aligned} \epsilon_{L-1}^* &= \epsilon_L^* \frac{d\mu_L}{dv_{L-1}^*} = (T - \mu_L^*) \frac{d\mu_L^*}{dv_{L-1}^*} \\ &= \frac{dL}{dv_L^*} \frac{d\mu_L^*}{dv_{L-1}^*} = \frac{dL}{dv_L^*} \frac{dv_L^*}{dv_{L-1}^*} \\ &= \frac{dL}{dv_{L-1}^*} \end{aligned} \quad (3)$$

In the first step we simply substitute $\epsilon_L = (T - \mu_L^*)$. On the second line we use the fact that $(T - \mu_L) = \frac{dL}{dv_L^*}$ and that $\frac{d\mu_L^*}{dv_{L-1}^*} = \frac{dv_L^*}{dv_{L-1}^*}$ which in this case follows trivially since v_L^* has no children. The final line is just recognising that this is the correct backpropagated gradient by the chain rule. We recurse backwards through the graph to a parent $v_{L-2} \in \text{Par}(v_{L-1})$ of v_{L-1} . Here some additional subtlety is needed since v_{L-2} may have many children which each contribute to the loss. Fortunately these different paths sum together at the node v_{L-2} , thus propagating the correct

³We assume here only a single output but the multi-output case is a straightforward generalisation.

gradient backwards.

$$\begin{aligned}
\epsilon_{L-2}^* &= \sum_{j=\text{Chi}(v_{L-2}^*)} \epsilon_j^* \frac{d\mu_j^*}{dv_{L-2}^*} \\
&= \sum_{j=\text{Chi}(v_{L-2}^*)} \frac{dL}{dv_j^*} \frac{dv_j^*}{d\mu_{L-1}^*} \\
&= \frac{dL}{dv_{L-2}^*}
\end{aligned}$$

Where in the second line we have used the fact that we already know that the equilibrium values of the child error units are their backpropagated gradient. We also know that $\frac{d\mu_j^*}{dv_{L-2}^*} = \frac{dv_j^*}{d\mu_{L-1}^*}$ since, by Equation 4, $v_i^* = \mu_i^* - \sum_{j=\text{Chi}(v_i)} \epsilon_j^* \frac{d\mu_j^*}{dv_j^*}$ and $\frac{d}{dv_i^*} [\sum_{j=\text{Chi}(\text{Chi}(v_i))} \epsilon_j^* \frac{d\mu_j^*}{dv_j^*}] = 0$ since the children of the child have no immediate dependence on the parent. Thus, by induction we have shown that the fixed points of the error units of the global optimization correspond exactly to the backpropagated gradients. Intuitively, if we imagine the computation-graph as a chain and the error as 'tension' in the chain, backprop loads all the tension at the end (the output) and then systematically propagates it backwards. Predictive coding, however spreads the tension throughout the entire chain until it reaches an equilibrium where the amount of tension at each link is precisely the backpropagated gradient.

Finally, suppose the edge-function, $f(x)$, at some vertex v_i has parameters θ_i which we wish to optimize. The dynamics of θ_i as a gradient descent on \mathcal{F} also exactly match the backpropagated parameter gradients.

$$\begin{aligned}
\frac{d\theta}{dt} &= -\frac{d\mathcal{F}}{d\theta} = \epsilon_i^* \frac{d\epsilon_i^*}{d\theta_i} \\
&= \frac{dL}{dv_i^*} \frac{dv_i^*}{d\theta_i} = \frac{dL}{d\theta_i}
\end{aligned} \tag{4}$$

Where in the second line we have used the fact that $\epsilon_i^* = \frac{dL}{dv_i^*}$ and that $\frac{d\epsilon_i^*}{d\theta_i} = \frac{d\mu_i}{d\theta_i}$ since $\epsilon_i = v_i - \mu_i$ and at equilibrium $\frac{d\mu_i}{d\theta_i} = \frac{dv_i^*}{d\theta_i}$ as shown above. In the special case of parameter-linear functions which consist of a linear superposition of parameters and vertex values followed by a nonlinear function – i.e. $\mu_{i+1} = f(\theta_i^T v_i)$, as is standard in most machine learning architectures, then we obtain that $\frac{d\theta_i}{dt} = \frac{dL}{dv_i^*} \frac{dv_i^*}{d\theta_i} = \epsilon_i^* \frac{df(\theta_i^T v_i)}{d\theta_i} v_i^{*T}$ which is a Hebbian learning rule as it is simply a component-wise multiplication of the prediction errors of the child with the activations of the parent weighted by the derivative of the activation function.

5 Results

5.1 Numerical Results

To demonstrate the correctness of our derivation, we present a numerical test in the simple scalar case, where we use predictive coding to derive the gradients of an arbitrary, highly nonlinear test function $v_L = \tan(\sqrt{\theta}v_0) + \sin(v_0^2)$ where θ is an arbitrary parameter. For our tests we set v_0 to 5 and θ to 2. The computation graph for this function is presented in Figure 1. Although simple, this is a good test of predictive coding because the function is highly nonlinear, and also its computation graph does not follow a simple layer structure but includes some branching. An arbitrary target of $T = 3$ was set at the output and the gradient of the loss $L = (v_L - T)^2$ with respect to the input v_0 was computed using predictive coding. We show (Figure 2) that the predictive coding optimisation rapidly converges to the exact numerical gradients computed by automatic differentiation (using PyTorch (Paszke et al., 2017)), and that moreover this optimization is very robust and can handle even exceptionally high learning rates (up to 0.5) without divergence. We explore the interesting properties of the variational, or "inner-loop" optimization in Appendix E.

In sum, we have shown and numerically verified that at the equilibrium point of the global free-energy \mathcal{F} on an arbitrary computation graph, the error units exactly equal the backpropagated gradients, and that this descent requires only local connectivity, does not require a separate phases or a sequential backwards sweep, and in the case of parameter-linear

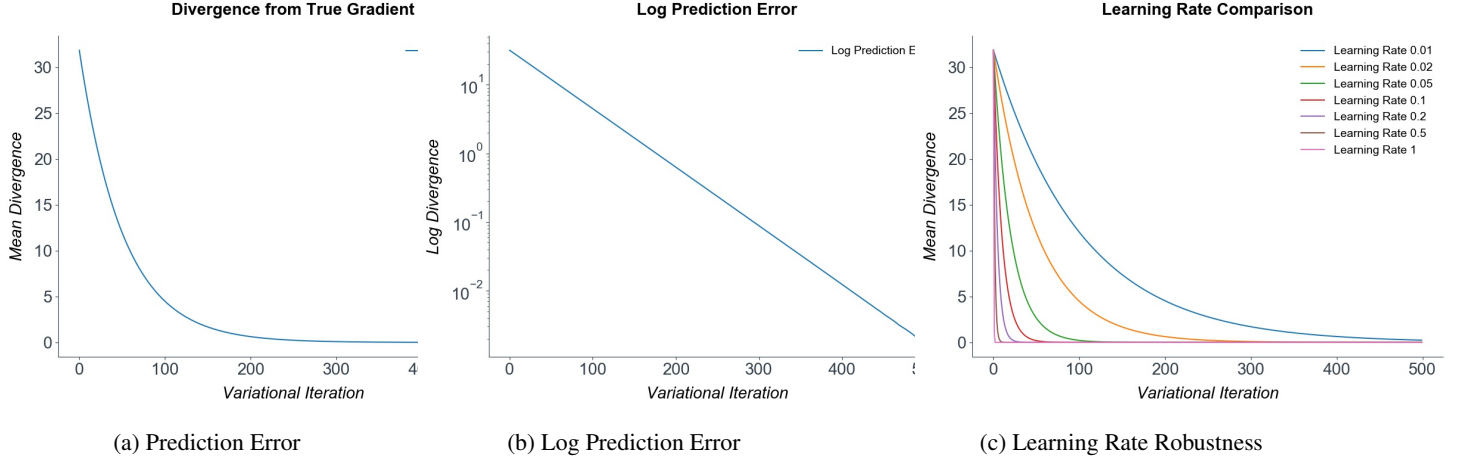


Figure 2: Prediction error decreases exponentially on the test function directly to the global minimum. Moreover, the optimisation is highly stable and convergent even with extremely high learning rates.

functions, requires only Hebbian plasticity. Pseudocode and further discussion of the general algorithm is presented in Appendix A. Our results provide a straightforward recipe for the direct implementation of predictive coding algorithms to approximate certain computation graphs, such as those found in common machine learning algorithms, in a biologically plausible manner. Next, we showcase this capability by developing predictive coding variants of core machine learning architectures - convolutional neural networks (CNNs) recurrent neural networks (RNNs) and LSTMs (Hochreiter & Schmidhuber, 1997), and show performance comparable with backprop on tasks substantially more challenging than MNIST.⁴

5.2 Predictive Coding CNN

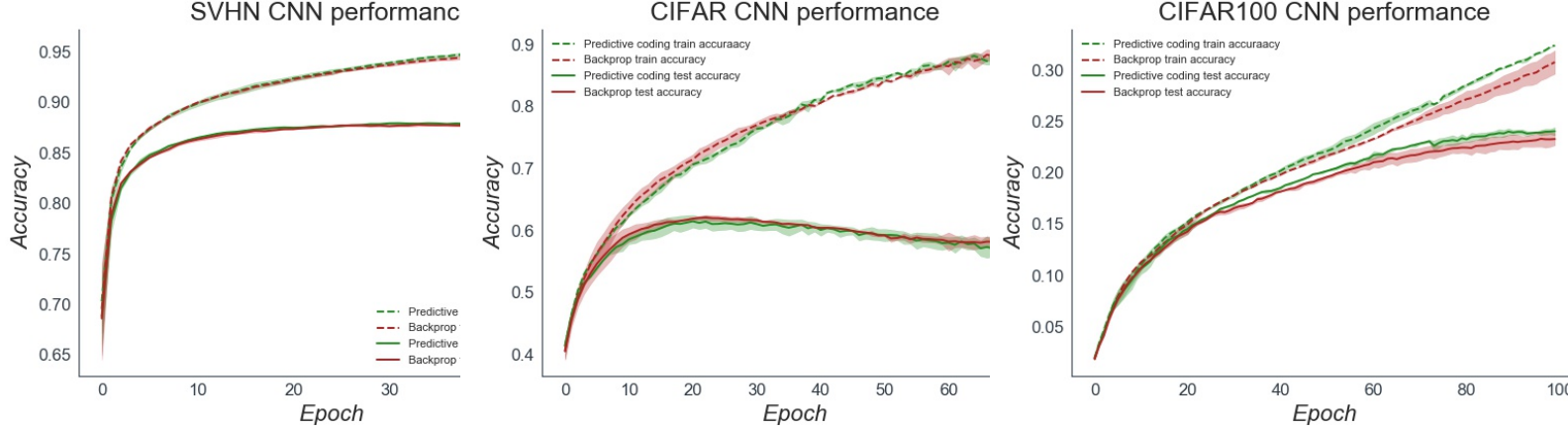


Figure 3: Training and test accuracy plots for the Predictive Coding and Backprop CNN on SVHN, CIFAR10, and CIFAR100 dataest over 5 seeds. Performance is largely indistinguishable. Due to the need to iterate the vs until convergence, the predictive coding network had roughly a 100x greater computational cost than the backprop network.

First we constructed predictive coding CNN models (see Appendix C for full implementation details). In the predictive coding CNN, each filter kernel was augmented with 'error maps' which measured the difference between the forward convolutional predictions and the backwards messages. Our CNN was composed of a convolutional layer, followed by a max-pooling layer, and then two further convolutional layers followed by 3 fully-connected layers. We compared our

⁴Code to reproduce all experiments and figures in this work can be found at <https://github.com/BerenMillidge/PredictiveCodingBackprop>

predictive coding CNN to a backprop-trained CNN with the exact same architecture and hyperparameters. We tested our models on three image classification datasets significantly more challenging than MNIST – SVHN, CIFAR10, and CIFAR100. SVHN is a digit recognition task like MNIST, but has more naturalistic backgrounds, is in colour with continuously varying inputs (rather than binary like MNIST) and contains distractor digits. CIFAR10 and CIFAR100 are large image datasets composed of RGB 32x32 images. CIFAR10 has 10 classes of image, while CIFAR100 is substantially more challenging with 100 possible classes. In general performance was identical between the predictive coding and backprop CNNs and comparable to the standard performance of basic CNN models on these datasets. Moreover, the predictive coding gradient remained close to the true numerical gradient throughout training (Appendix C).

5.3 Predictive Coding LSTM and RNN

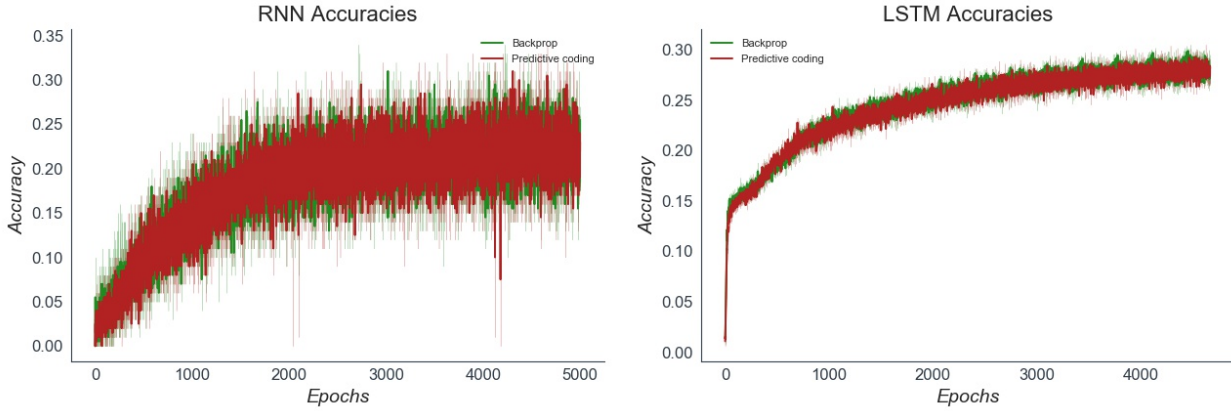


Figure 4: Test accuracy plots for the Predictive Coding and Backprop RNN and LSTM on their respective tasks, averaged over 5 seeds. Performance is again indistinguishable from backprop.

We also constructed predictive coding RNN and LSTM models, thus demonstrating the ability of predictive coding to scale to non-parameter-linear, branching, computation graphs. The RNN was trained on a character-level name classification task, while the LSTM was trained on a next-character prediction task on the full works of Shakespeare. Full implementation details can be found in Appendices C and D. LSTMs and RNNs are recurrent networks which are trained through backpropagation through time (BPTT). BPTT simply unrolls the network through time and backpropagates through the unrolled graph. Analogously we trained the predictive coding RNN and LSTM by applying predictive coding to the unrolled computation graph. The depth of the unrolled graph depends heavily on the sequence length, and in our tasks using a sequence length of 100 we still found that predictive coding evinced rapid convergence to the correct numerical gradient, thus showing that the algorithm is scalable even to very deep computation graphs.

6 Discussion

We have shown that predictive coding provides a local and often biologically plausible approximation to backprop on arbitrary, deep, and branching computation graphs. Moreover, convergence to the exact backprop gradients is rapid and robust, even in extremely deep graphs such as the unrolled LSTM. Our algorithm is fully parallelizable, does not require separate phases, and can produce equivalent performance to backprop in core machine-learning architectures. These results broaden the horizon of local approximations to backprop by demonstrating that they can be implemented on arbitrary computation graphs, not only simple MLP architectures. Our work prescribes a straightforward recipe for backpropagating through any computation graph with predictive coding using only local learning rules. In the future, this process could potentially be made fully automatic and translated onto neuromorphic hardware. Our results also raise the possibility that the brain may implement machine-learning type architectures much more directly than often

considered. Many lines of work suggest a close correspondence between the representations and activations of CNNs and activity in higher visual areas (Eickenberg, Gramfort, Varoquaux, & Thirion, 2017; Khaligh-Razavi & Kriegeskorte, 2014; Lindsay, 2020; Tacchetti, Isik, & Poggio, 2017; Yamins et al., 2014), for instance, and this similarity may be found to extend to other machine learning architectures.

Although we have implemented three core machine learning architectures as predictive coding networks, we have nevertheless focused on relatively small and straightforward networks and thus both our backprop and predictive coding networks perform below the state of the art on the presented tasks. This is primarily because our focus was on demonstrating the theoretical convergence between the two algorithms. Nevertheless, we believe that due to the generality of our theoretical results, ‘scaling up’ the existing architectures to implement performance-matched predictive coding versions of more advanced machine learning architectures such as resnets (He, Zhang, Ren, & Sun, 2016), GANs (Goodfellow et al., 2014), and transformers (Vaswani et al., 2017) should be relatively straightforward.

In terms of computational cost, one inference iteration in the predictive coding network is about as costly as a backprop backwards pass. Thus, due to using 100-200 iterations for full convergence, our algorithm is substantially more expensive than backprop which limits the scalability of our method. However, this serial cost is misleading when talking about highly parallel neural architectures. In the brain, neurons cannot wait for a sequential forward and backward sweep. By phrasing our algorithm as a global descent, our algorithm is fully parallel across layers. There is no waiting and no phases to be coordinated. Each neuron need only respond to its local driving inputs and downwards error signals. We believe that this local and parallelizable property of our algorithm may engender the possibility of substantially more efficient implementations on neuromorphic hardware (Davies et al., 2018; Furber, Galluppi, Temple, & Plana, 2014; Merolla et al., 2014), which may ameliorate much of the computational overhead compared to backprop. Future work could also examine whether our method is more capable than backprop of handling the continuously varying inputs the brain is presented with in practice, rather than the artificial paradigm of being presented with a series of *i.i.d.* datapoints.

Our work also reveals a close connection between backprop and inference. Namely, the recursive computation of gradients is effectively a by-product of a variational-inference algorithm which infers the values of the vertices of the computation graph under a hierarchical Gaussian generative model. While the deep connections between stochastic gradient descent and inference in terms of Kalman filtering (Ollivier, 2019; Ruck, Rogers, Kabrisky, Maybeck, & Oxley, 1992) or MCMC sampling methods (T. Chen, Fox, & Guestrin, 2014; Mandt, Hoffman, & Blei, 2017) is known, the relation between recursive gradient computation itself and variational inference is underexplored. Our method can provide a principled generalisation of backprop through the inverse-variance Σ^{-1} parameters of the Gaussian generative model. These parameters weight the relative contribution of different factors to the overall gradient by their uncertainty, thus naturally handling the case of backprop with differentially noisy inputs. Moreover, the Σ^{-1} parameters can be learnt as a gradient descent on \mathcal{F} : $\frac{d\Sigma_i}{dt} = -\frac{d\mathcal{F}}{d\Sigma_i} = -\Sigma_i^{-1}\epsilon_i\epsilon_i^T\Sigma_i^{-1} - \Sigma_i^{-1}$. This specific generalisation is afforded by the Gaussian form of the generative model, however, and other generative models may yield novel optimisation algorithms able to quantify and handle uncertainties throughout the entire computational graph.

Acknowledgements

BM is supported by an EPSRC funded PhD Studentship. AT is funded by a PhD studentship from the Dr. Mortimer and Theresa Sackler Foundation and the School of Engineering and Informatics at the University of Sussex. CLB is supported by BBRSC grant number BB/P022197/1. AT is grateful to the Dr. Mortimer and Theresa Sackler Foundation, which supports the Sackler Centre for Consciousness Science. The authors would also like to thank Anil Seth and Manuel Baltieri for their helpful comments and discussions relating to the manuscript.

Broader Impact

Our work shows that predictive coding can approximate backprop in machine learning architectures with only local learning rules. Since the predictive coding algorithm only performs as well as backprop, and with substantial computational overhead, the short-term interest of this fact is primarily theoretical and we do not foresee any immediate societal effects, positive or negative. In the longer-term, our research may be utilised to translate powerful machine learning algorithms to neuromorphic architectures which could, in theory, potentially lead to significantly more energy-efficient machine learning hardware and may have implications for some applications such as IoT devices. If current trends continue, greater ubiquity and energy-efficiency of machine learning systems in small neuromorphic devices will likely lead to greater convenience for consumers at the expense of industrial consolidation and erosion of privacy. Our work may also aid understanding the intersection of current deep learning architectures and the brain, which may potentially lead to a greater understanding of biological intelligence, and improvements in the development of biologically-inspired artificial intelligence. Over the longer term, predicting whether this is beneficial on-net is challenging.

References

Akrout, M., Wilson, C., Humphreys, P., Lillicrap, T., & Tweed, D. B. (2019). Deep learning without weight transport. In *Advances in neural information processing systems* (pp. 974–982).

Amit, Y. (2019). Deep learning with asymmetric connections and hebbian updates. *Frontiers in computational neuroscience*, 13, 18.

Amos, B., & Yarats, D. (2019). The differentiable cross-entropy method. *arXiv preprint arXiv:1909.12830*.

Auksztulewicz, R., & Friston, K. (2016). Repetition suppression and its contextual determinants in predictive coding. *cortex*, 80, 125–140.

Bastos, A. M., Usrey, W. M., Adams, R. A., Mangun, G. R., Fries, P., & Friston, K. J. (2012). Canonical microcircuits for predictive coding. *Neuron*, 76(4), 695–711.

Baydin, A. G., Pearlmutter, B. A., Radul, A. A., & Siskind, J. M. (2017). Automatic differentiation in machine learning: a survey. *The Journal of Machine Learning Research*, 18(1), 5595–5637.

Beal, M. J., et al. (2003). *Variational algorithms for approximate bayesian inference*. university of London London.

Bengio, Y., & Fischer, A. (2015). Early inference in energy-based models approximates back-propagation. *arXiv preprint arXiv:1510.02777*.

Bengio, Y., Mesnard, T., Fischer, A., Zhang, S., & Wu, Y. (2017). Stdः-compatible approximation of backpropagation in an energy-based model. *Neural computation*, 29(3), 555–577.

Blei, D. M., Kucukelbir, A., & McAuliffe, J. D. (2017). Variational inference: A review for statisticians. *Journal of the American statistical Association*, 112(518), 859–877.

Bogacz, R. (2017). A tutorial on the free-energy framework for modelling perception and learning. *Journal of mathematical psychology*, 76, 198–211.

Boyd, S., Boyd, S. P., & Vandenberghe, L. (2004). *Convex optimization*. Cambridge university press.

Buckley, C. L., Kim, C. S., McGregor, S., & Seth, A. K. (2017). The free energy principle for action and perception: A mathematical review. *Journal of Mathematical Psychology*, 81, 55–79.

Bullier, J. (2001). Integrated model of visual processing. *Brain research reviews*, 36(2-3), 96–107.

Chen, T., Fox, E., & Guestrin, C. (2014). Stochastic gradient hamiltonian monte carlo. In *International conference on machine learning* (pp. 1683–1691).

Chen, T. Q., Rubanova, Y., Bettencourt, J., & Duvenaud, D. K. (2018). Neural ordinary differential equations. In *Advances in neural information processing systems* (pp. 6571–6583).

Crick, F. (1989). The recent excitement about neural networks. *Nature*, 337(6203), 129–132.

Davies, M., Srinivasa, N., Lin, T.-H., Chinya, G., Cao, Y., Choday, S. H., ... others (2018). Loihi: A neuromorphic manycore processor with on-chip learning. *IEEE Micro*, 38(1), 82–99.

Degrave, J., Hermans, M., Dambre, J., & Wyffels, F. (2019). A differentiable physics engine for deep learning in robotics. *Frontiers in neurorobotics*, 13, 6.

Eickenberg, M., Gramfort, A., Varoquaux, G., & Thirion, B. (2017). Seeing it all: Convolutional network layers map the function of the human visual system. *NeuroImage*, 152, 184–194.

Feldman, H., & Friston, K. (2010). Attention, uncertainty, and free-energy. *Frontiers in human neuroscience*, 4, 215.

Friston, K. (2003). Learning and inference in the brain. *Neural Networks*, 16(9), 1325–1352.

Friston, K. (2005). A theory of cortical responses. *Philosophical transactions of the Royal Society B: Biological sciences*, 360(1456), 815–836.

Friston, K. (2008). Hierarchical models in the brain. *PLoS computational biology*, 4(11).

Furber, S. B., Galluppi, F., Temple, S., & Plana, L. A. (2014). The spinnaker project. *Proceedings of the IEEE*, 102(5), 652–665.

Goodfellow, I., Pouget-Abadie, J., Mirza, M., Xu, B., Warde-Farley, D., Ozair, S., ... Bengio, Y. (2014). Generative adversarial nets. In *Advances in neural information processing systems* (pp. 2672–2680).

Griewank, A., et al. (1989). On automatic differentiation. *Mathematical Programming: recent developments and applications*, 6(6), 83–107.

Guerguiev, J., Lillicrap, T. P., & Richards, B. A. (2017). Towards deep learning with segregated dendrites. *Elife*, 6, e22901.

Hassabis, D., Kumaran, D., Summerfield, C., & Botvinick, M. (2017). Neuroscience-inspired artificial intelligence. *Neuron*, 95(2), 245–258.

Hawkins, J., & Blakeslee, S. (2007). *On intelligence: How a new understanding of the brain will lead to the creation of truly intelligent machines*. Macmillan.

He, K., Zhang, X., Ren, S., & Sun, J. (2016). Deep residual learning for image recognition. In *Proceedings of the ieee conference on computer vision and pattern recognition* (pp. 770–778).

Heiden, E., Millard, D., & Sukhatme, G. (2019). Real2sim transfer using differentiable physics. In *Workshop on closing the reality gap in sim2real transfer for robotic manipulation*.

Hochreiter, S., & Schmidhuber, J. (1997). Long short-term memory. *Neural computation*, 9(8), 1735–1780.

Hohwy, J., Roepstorff, A., & Friston, K. (2008). Predictive coding explains binocular rivalry: An epistemological review. *Cognition*, 108(3), 687–701.

Hung, C. P., Kreiman, G., Poggio, T., & DiCarlo, J. J. (2005). Fast readout of object identity from macaque inferior temporal cortex. *Science*, 310(5749), 863–866.

Innes, M., Edelman, A., Fischer, K., Rackauckus, C., Saba, E., Shah, V. B., & Tebbutt, W. (2019). Zygote: A differentiable programming system to bridge machine learning and scientific computing. *arXiv preprint arXiv:1907.07587*.

Kanai, R., Komura, Y., Shipp, S., & Friston, K. (2015). Cerebral hierarchies: predictive processing, precision and the pulvinar. *Philosophical Transactions of the Royal Society B: Biological Sciences*, 370(1668), 20140169.

Kaplan, J., McCandlish, S., Henighan, T., Brown, T. B., Chess, B., Child, R., ... Amodei, D. (2020). Scaling laws for neural language models. *arXiv preprint arXiv:2001.08361*.

Khaligh-Razavi, S.-M., & Kriegeskorte, N. (2014). Deep supervised, but not unsupervised, models may explain it cortical representation. *PLoS computational biology*, 10(11).

Krizhevsky, A., Sutskever, I., & Hinton, G. E. (2012). Imagenet classification with deep convolutional neural networks. In *Advances in neural information processing systems* (pp. 1097–1105).

Lamme, V. A., & Roelfsema, P. R. (2000). The distinct modes of vision offered by feedforward and recurrent processing. *Trends in neurosciences*, 23(11), 571–579.

Lee, D.-H., Zhang, S., Fischer, A., & Bengio, Y. (2015). Difference target propagation. In *Joint european conference on machine learning and knowledge discovery in databases* (pp. 498–515).

Liao, Q., Leibo, J. Z., & Poggio, T. (2016). How important is weight symmetry in backpropagation? In *Thirtieth aaai conference on artificial intelligence*.

Lillicrap, T. P., Cownden, D., Tweed, D. B., & Akerman, C. J. (2016). Random synaptic feedback weights support error backpropagation for deep learning. *Nature communications*, 7(1), 1–10.

Lillicrap, T. P., & Santoro, A. (2019). Backpropagation through time and the brain. *Current opinion in neurobiology*, 55, 82–89.

Lillicrap, T. P., Santoro, A., Marris, L., Akerman, C. J., & Hinton, G. (2020). Backpropagation and the brain. *Nature Reviews Neuroscience*, 1–12.

Lindsay, G. (2020). Convolutional neural networks as a model of the visual system: past, present, and future. *Journal of Cognitive Neuroscience*, 1–15.

Lotter, W., Kreiman, G., & Cox, D. (2016). Deep predictive coding networks for video prediction and unsupervised learning. *arXiv preprint arXiv:1605.08104*.

Mandt, S., Hoffman, M. D., & Blei, D. M. (2017). Stochastic gradient descent as approximate bayesian inference. *The Journal of Machine Learning Research*, 18(1), 4873–4907.

Merolla, P. A., Arthur, J. V., Alvarez-Icaza, R., Cassidy, A. S., Sawada, J., Akopyan, F., ... others (2014). A million spiking-neuron integrated circuit with a scalable communication network and interface. *Science*, 345(6197), 668–673.

Mnih, V., Kavukcuoglu, K., Silver, D., Rusu, A. A., Veness, J., Bellemare, M. G., ... others (2015). Human-level control through deep reinforcement learning. *Nature*, 518(7540), 529–533.

Okada, M., Rigazio, L., & Aoshima, T. (2017). Path integral networks: End-to-end differentiable optimal control. *arXiv preprint arXiv:1706.09597*.

Ollivier, Y. (2019). The extended kalman filter is a natural gradient descent in trajectory space. *arXiv preprint arXiv:1901.00696*.

Ollivier, Y., Tallec, C., & Charpiat, G. (2015). Training recurrent networks online without backtracking. *arXiv preprint arXiv:1507.07680*.

Ororbia, A., Mali, A., Giles, C. L., & Kifer, D. (2020). Continual learning of recurrent neural networks by locally aligning distributed representations. *IEEE Transactions on Neural Networks and Learning Systems*.

Pal, A. (2019). Raytracer. jl: A differentiable renderer that supports parameter optimization for scene reconstruction. *arXiv preprint arXiv:1907.07198*.

Paszke, A., Gross, S., Chintala, S., Chanan, G., Yang, E., DeVito, Z., ... Lerer, A. (2017). Automatic differentiation in pytorch.

Rackauckas, C., Innes, M., Ma, Y., Bettencourt, J., White, L., & Dixit, V. (2019). Diffeqflux. jl-a julia library for neural differential equations. *arXiv preprint arXiv:1902.02376*.

Radford, A., Wu, J., Child, R., Luan, D., Amodei, D., & Sutskever, I. (2019). Language models are unsupervised multitask learners. *OpenAI Blog*, 1(8), 9.

Rao, R. P., & Ballard, D. H. (1999). Predictive coding in the visual cortex: a functional interpretation of some extra-classical receptive-field effects. *Nature neuroscience*, 2(1), 79–87.

Revels, J., Lubin, M., & Papamarkou, T. (2016). Forward-mode automatic differentiation in julia. *arXiv preprint arXiv:1607.07892*.

Richards, B. A., Lillicrap, T. P., Beaudoin, P., Bengio, Y., Bogacz, R., Christensen, A., ... others (2019). A deep learning framework for neuroscience. *Nature neuroscience*, 22(11), 1761–1770.

Ruck, D. W., Rogers, S. K., Kabrisky, M., Maybeck, P. S., & Oxley, M. E. (1992). Comparative analysis of backpropagation and the extended kalman filter for training multilayer perceptrons. *IEEE Transactions on Pattern Analysis & Machine Intelligence*(6), 686–691.

Sacramento, J., Costa, R. P., Bengio, Y., & Senn, W. (2018). Dendritic cortical microcircuits approximate the backpropagation algorithm. In *Advances in neural information processing systems* (pp. 8721–8732).

Scellier, B., & Bengio, Y. (2017). Equilibrium propagation: Bridging the gap between energy-based models and backpropagation. *Frontiers in computational neuroscience*, 11, 24.

Scellier, B., Goyal, A., Binas, J., Mesnard, T., & Bengio, Y. (2018). Generalization of equilibrium propagation to vector

field dynamics. *arXiv preprint arXiv:1808.04873*.

Schrittwieser, J., Antonoglou, I., Hubert, T., Simonyan, K., Sifre, L., Schmitt, S., ... others (2019). Mastering atari, go, chess and shogi by planning with a learned model. *arXiv preprint arXiv:1911.08265*.

Serre, T., Oliva, A., & Poggio, T. (2007). A feedforward architecture accounts for rapid categorization. *Proceedings of the national academy of sciences*, 104(15), 6424–6429.

Seung, H. S. (2003). Learning in spiking neural networks by reinforcement of stochastic synaptic transmission. *Neuron*, 40(6), 1063–1073.

Shipp, S. (2016). Neural elements for predictive coding. *Frontiers in psychology*, 7, 1792.

Silver, D., Schrittwieser, J., Simonyan, K., Antonoglou, I., Huang, A., Guez, A., ... others (2017). Mastering the game of go without human knowledge. *Nature*, 550(7676), 354–359.

Spratling, M. W. (2008). Reconciling predictive coding and biased competition models of cortical function. *Frontiers in computational neuroscience*, 2, 4.

Steil, J. J. (2004). Backpropagation-decorrelation: online recurrent learning with $O(n)$ complexity. In *2004 ieee international joint conference on neural networks (ieee cat. no. 04ch37541)* (Vol. 2, pp. 843–848).

Szegedy, C., Liu, W., Jia, Y., Sermanet, P., Reed, S., Anguelov, D., ... Rabinovich, A. (2015). Going deeper with convolutions. In *Proceedings of the ieee conference on computer vision and pattern recognition* (pp. 1–9).

Tacchetti, A., Isik, L., & Poggio, T. (2017). Invariant recognition drives neural representations of action sequences. *PLoS computational biology*, 13(12), e1005859.

Tallec, C., & Ollivier, Y. (2017). Unbiased online recurrent optimization. *arXiv preprint arXiv:1702.05043*.

Tzen, B., & Raginsky, M. (2019). Neural stochastic differential equations: Deep latent gaussian models in the diffusion limit. *arXiv preprint arXiv:1905.09883*.

VanRullen, R. (2007). The power of the feed-forward sweep. *Advances in Cognitive Psychology*, 3(1-2), 167.

Vaswani, A., Shazeer, N., Parmar, N., Uszkoreit, J., Jones, L., Gomez, A. N., ... Polosukhin, I. (2017). Attention is all you need. In *Advances in neural information processing systems* (pp. 5998–6008).

Vinyals, O., Babuschkin, I., Czarnecki, W. M., Mathieu, M., Dudzik, A., Chung, J., ... others (2019). Grandmaster level in starcraft ii using multi-agent reinforcement learning. *Nature*, 575(7782), 350–354.

Watanabe, E., Kitaoka, A., Sakamoto, K., Yasugi, M., & Tanaka, K. (2018). Illusory motion reproduced by deep neural networks trained for prediction. *Frontiers in psychology*, 9, 345.

Weilnhammer, V., Stuke, H., Hesselmann, G., Sterzer, P., & Schmack, K. (2017). A predictive coding account of bistable perception-a model-based fmri study. *PLoS computational biology*, 13(5), e1005536.

Werbos, P. J. (1982). Applications of advances in nonlinear sensitivity analysis. In *System modeling and optimization* (pp. 762–770). Springer.

Whittington, J. C., & Bogacz, R. (2017). An approximation of the error backpropagation algorithm in a predictive coding network with local hebbian synaptic plasticity. *Neural computation*, 29(5), 1229–1262.

Whittington, J. C., & Bogacz, R. (2019). Theories of error back-propagation in the brain. *Trends in cognitive sciences*.

Williams, R. J., & Zipser, D. (1989). A learning algorithm for continually running fully recurrent neural networks. *Neural computation*, 1(2), 270–280.

Yamins, D. L., Hong, H., Cadieu, C. F., Solomon, E. A., Seibert, D., & DiCarlo, J. J. (2014). Performance-optimized hierarchical models predict neural responses in higher visual cortex. *Proceedings of the National Academy of Sciences*, 111(23), 8619–8624.

Appendix A: General Algorithm

Given a general computation graph $\mathcal{G} = \{\mathbb{E}, \mathbb{V}\}$, predictive coding first adds error units $\epsilon \in \mathcal{E}$ to the graph to obtain an augmented computation graph $\tilde{\mathcal{G}} = \{\mathbb{E}, \mathbb{V}, \mathcal{E}\}$, and the connectivity is rewired such that the connection between parent and child in the original computation graph is between the parent and the error unit, which is then connected to

the child, so that it computes the difference between the child and the prediction of the parents. The predictive coding algorithm is applied to this augmented graph.

First the augmented computation graph is run forwards so that each set of parents computes its predictions, all the way to the output. The prediction at the output is compared to the target and this sets the output prediction errors.

Then a global descent occurs in which the values of every vertex and every error unit is updated in parallel according to Equation 2, until the vertex values converge to the minimum of the free-energy.

At equilibrium, the error units should have converged to the exact backpropagated gradients, and then these are used to update the parameters in a way that exactly mimics the true backprop update.

Algorithm 1: Generalized Predictive Coding

Data: Dataset $\mathcal{D} = \{\mathbf{X}, \mathbf{L}\}$, Augmented Computation Graph $\tilde{\mathcal{G}} = \{\mathbb{E}, \mathbb{V}, \mathcal{E}\}$, inference learning rate η_v , weight learning rate η_θ

begin

```

/* For each minibatch in the dataset */  

for  $(x, L) \in \mathcal{D}$  do  

    /* Fix start of graph to inputs */  

     $v_0 \leftarrow x$   

    /* Forward pass to compute predictions */  

    for  $v_i \in \mathbb{V}$  do  

         $\mu_i \leftarrow f(\text{Par}(v_i); \theta)$   

    /* Compute output error */  

     $\epsilon_L \leftarrow L - \mu_L$   

    /* Begin inner descent on the free-energy */  

    while not converged do  

        for  $(v_i, \epsilon_i) \in \tilde{\mathcal{G}}$  do  

            /* Compute prediction errors */  

             $\epsilon_i \leftarrow v_i - \mu_i$   

            /* Update the vertex values */  

             $v_i^{t+1} \leftarrow v_i^t + \eta_v \frac{d\mathcal{F}}{dv_i^t}$   

        /* Update weights at equilibrium */  

        for  $\theta_i \in \mathbb{E}$  do  

             $\theta_i^{t+1} \leftarrow \theta_i^t + \eta_\theta \frac{d\mathcal{F}}{d\theta_i^t}$ 

```

In this work, we initialized the vertices as a direct function of their parents $v_i^0 = f(\text{Par}(v_i^0))$. This was necessary to obtain exact convergence to the numerical gradients of the equivalent backprop neural network since, for the loss, and hence the gradients, to match, the initial output μ_L^{PC} must equal the output of the backprop network μ_L^{BP} . Neurally, this could correspond to an initial feedforward sweep, for which there is substantial evidence in the brain (Bullier, 2001; Hung, Kreiman, Poggio, & DiCarlo, 2005; Lamme & Roelfsema, 2000; Serre, Oliva, & Poggio, 2007; VanRullen, 2007). Although required to exactly match the backprop gradients, this initialization is not required for good performance. We will investigate this further in future work.

To translate the inner optimisation from continuous to discrete time we used a simple Euler integration scheme so that the update rule for the vertices became

$$v_i^{t+1} \leftarrow v_i^t - \eta \frac{d\mathcal{F}}{dv_i^t}$$

where η is the step-size parameter which in practice functions as a learning rate. Since this inner descent is primary cause of the computational overhead of the algorithm compared to backprop, we investigate its properties in detail in Appendix E. In general, we found that this optimisation is surprisingly robust and can successfully converge even with high learning rates. Because of this we used $\eta_v = 0.1$ for all simulations in this paper. We used a similar Euler-discretisation of the update rules for the weights. In this case, η_θ was set to be identical with the learning rate used in the backprop network, which was set to the value of 0.0001.

Appendix B: Predictive Coding CNN Implementation Details

The key concept in a CNN is that of an image convolution, where a small weight matrix is 'slid' (or convolved) across an image to produce an output image. Each patch of the output image only depends on a relatively small patch of the input image. Moreover, the weights of the filter stay the same during the convolution, so each pixel of the output image is generated using the same weights. The weight sharing implicit in the convolution operation enforces translational invariance, since different image patches are all processed with the same weights.

The forward equations of a convolutional layer for a specific output pixel

$$y_{i,j} = \sum_{k=i-f}^{k=i+f} \sum_{l=j-f}^{l=j+f} \theta_{k,l} x_{i+k, j+l}$$

Where $y_{i,j}$ is the (i, j) th element of the output, $x_{i,j}$ is the element of the input image and $\theta_{k,l}$ is an weight element of a feature map. To setup a predictive coding CNN, we augment each intermediate x_i and y_i with error units ϵ_i of the same dimension as the output of the convolutional layer.

Predictions μ are projected forward using the forward equations. Prediction errors also need to be transmitted backwards for the architecture to work. To achieve this we must have that prediction errors are transmitted upwards by a 'backwards convolution'. We thus define the backwards prediction errors $\hat{\epsilon}_j$ as follows:

$$\hat{\epsilon}_{i,j} = \sum_{k=i-f}^{i+f} \sum_{l=j-f}^{j+f} \theta_{j,i} \tilde{\epsilon}_{i,j}$$

Where $\tilde{\epsilon}$ is an error map zero-padded to ensure the correct convolutional output size. Inference in the predictive coding network then proceeds by updating the intermediate values of each layer as follows:

$$\frac{dy_l}{dt} = \epsilon_l - \hat{\epsilon}_{l+1}$$

Since the CNN is also parameter-linear, weights can be updated using the simple hebbian rule of the multiplication of the pre and post synaptic potentials.

$$\frac{d\theta_l}{dt} = \sum_{i,j} \epsilon_{l,i} y_{i,j}^{l-1T}$$

There is an additional biological implausibility here due to the weight sharing of the CNN. Since the same weights are copied for each position on the image, the weight updates have contributions from all aspects of the image simultaneously which violates the locality condition. A simple fix for this, which makes the network scheme plausible is to simply give each position on the image a filter with separate weights, thus removing the weight sharing implicit in the CNN. In effect this gives each patch of pixels a local receptive field with its own set of weights. The performance and scalability of such a locally connected predictive coding architecture would be an interesting avenue for future work, as this architecture has substantial homologies with the structure of the visual cortex.

In our experiments we used a relatively simple CNN architecture consisting of one convolutional layer of kernel size 5, and a filter bank of 6 filters. This was followed by a max-pooling layer with a (2,2) kernel and a further convolutional layer with a (5,5) kernel and filter bank of 16 filters. This was then followed by three fully connected layers of 200, 150, and 10 (or 100 for CIFAR100) output units. Although this architecture is far smaller than state of the art for

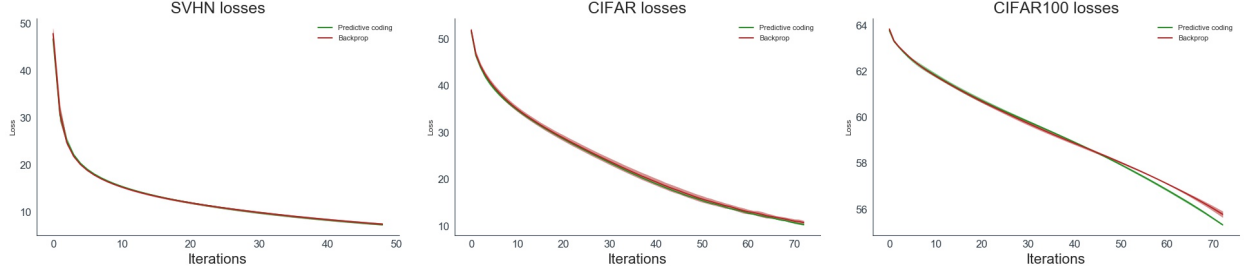


Figure 5: Training loss plots for the Predictive Coding and Backprop CNN on SVHN, CIFAR10, and CIFAR100 datasets over 5 seeds.

convolutional networks, the primary point of our paper was to demonstrate the equivalence of predictive coding and backprop. Further work could investigate scaling up predictive coding to more state-of-the-art architectures.

Our datasets consisted of 32x32 RGB images. We normalised the values of all pixels of each image to lie between 0 and 1, but otherwise performed no other image preprocessing. We did not use data augmentation of any kind. We set the weight learning rate for the predictive coding and backprop networks 0.0001. A minibatch size of 64 was used. These parameters were chosen without any detailed hyperparameter search and so are likely suboptimal. The magnitude of the gradient updates was clamped to lie between -50 and 50 in all of our models. This was done to prevent divergences, as occasionally occurred in the LSTM networks, likely due to exploding gradients.

The predictive coding scheme converged to the exact backprop gradients very precisely within 100 inference iterations using an inference learning rate of 0.1. This gives the predictive coding CNN approximately a 100x computational overhead compared to backprop. The divergence between the true and approximate gradients remained approximately constant throughout training, as shown by Figure 6, which shows the mean divergence for each layer of the CNN over the course of an example training run on the CIFAR10 dataset. The training loss of the predictive coding and backprop networks for SVHN, CIFAR10 and CIFAR100 are presented in Figure 5

Appendix C: Predictive Coding RNN

The computation graph on RNNs is relatively straightforward. We consider only a single layer RNN here although the architecture can be straightforwardly extended to hierarchically stacked RNNs. An RNN is similar to a feedforward network except that it possesses an additional hidden state h which is maintained and updated over time as a function of both the current input x and the previous hidden state. The output of the network y is a function of h . By considering the RNN at a single timestep we obtain the following equations.

$$\begin{aligned} h_t &= f(\theta_h h_{t-1} + \theta_x x_t) \\ y_t &= g(\theta_y h_t) \end{aligned} \tag{5}$$

Where f and g are elementwise nonlinear activation functions. And $\theta_h, \theta_x, \theta_y$ are weight matrices for each specific input. To predict a sequence the RNN simply rolls forward the above equations to generate new predictions and hidden states at each timestep.

RNNs are typically trained through an algorithm called backpropagation through time (BPTT) which essentially just unrolls the RNN into a single feedforward computation graph and then performs backpropagation through this unrolled graph. To train the RNN using predictive coding we take the same approach and simply apply predictive coding to the unrolled graph.

It is important to note that this is an additional aspect of biological implausibility that we do not address in this paper. BPTT requires updates to proceed backwards through time from the end of the sequence to the beginning. Ignoring any biological implausibility with the rules themselves, this updating sequence is clearly not biologically plausible as naively it requires maintaining the entire sequence of predictions and prediction errors perfectly in memory until the

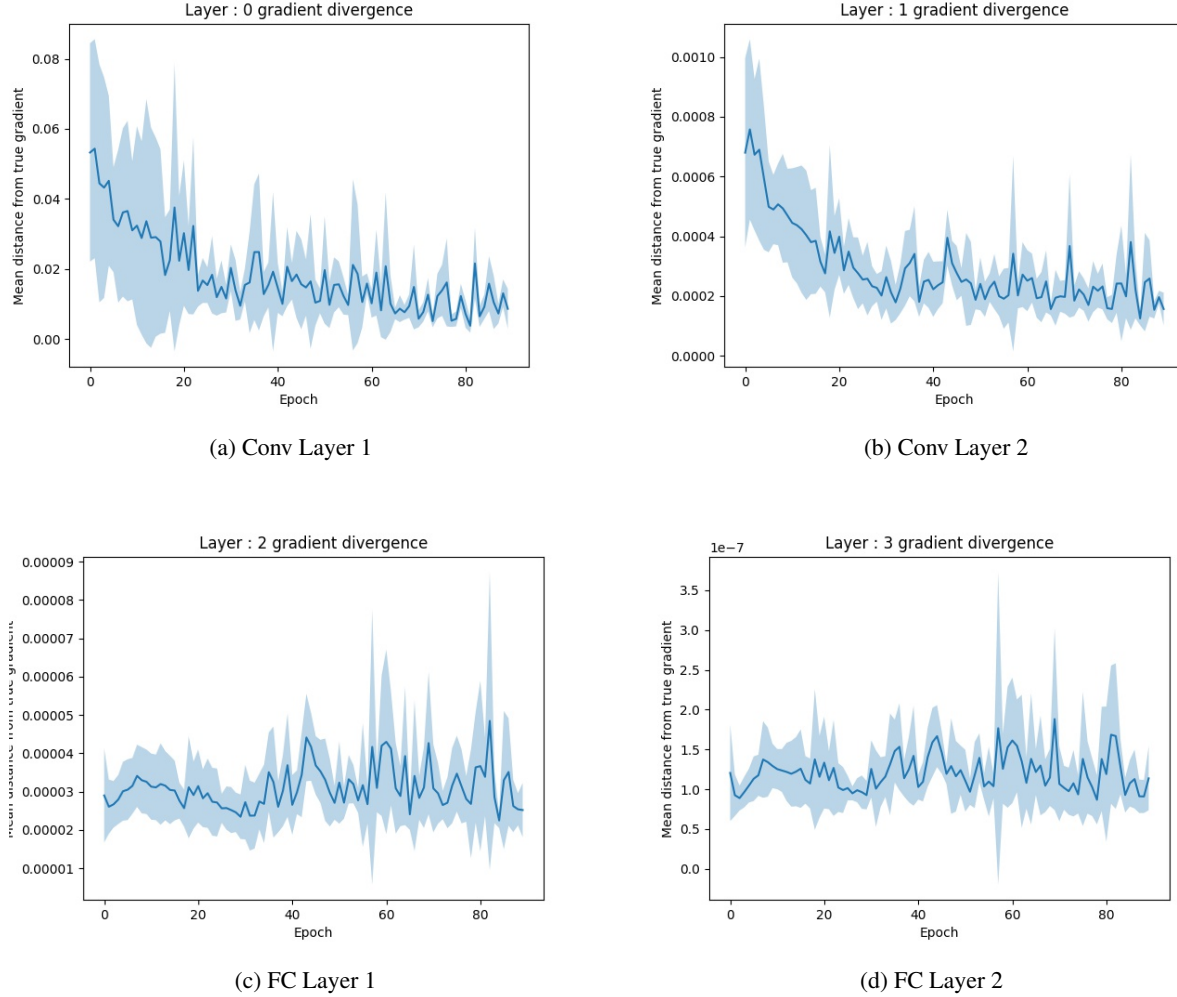


Figure 6: Mean divergence between the true numerical and predictive coding backprops over the course of training. In general, the divergence appeared to follow a largely random walk pattern, and was generally negligible. Importantly, the divergence did not grow over time throughout training, implying that errors from slightly incorrect gradients did not appear to compound.

end of the sequence, and waiting until the sequence ends before making any updates. There is a small literature on trying to produce biologically plausible, or forward-looking approximations to BPTT which does not require updates to be propagated back through time (Lillicrap & Santoro, 2019; Ollivier, Tallec, & Charpiat, 2015; Steil, 2004; Tallec & Ollivier, 2017; Williams & Zipser, 1989). While this is a fascinating area, we do not address it in this paper. We are solely concerned with the fact that predictive coding approximates backpropagation on feedforward computation graphs for which the unrolled RNN graph is a sufficient substrate.

To learn a predictive coding RNN, we first augment each of the variables h_t and y_t of the original graph with additional error units ϵ_{h_t} and ϵ_{y_t} . Predictions μ_{h_t}, μ_{y_t} are generated according to the feedforward rules (16). A sequence of true labels $\{T_1 \dots T_T\}$ is then presented to the network, and then inference proceeds by recursively applying the following

rules backwards through time until convergence.

$$\begin{aligned}\epsilon_{y_t} &= L - \mu_{y_t} \\ \epsilon_{h_t} &= h_t - \mu_{h_t} \\ \frac{dh_t}{dt} &= \epsilon_{h_t} - \epsilon_{y_t} \theta_y^T - \epsilon_{h_{t+1}} \theta_h^T\end{aligned}$$

Upon convergence the weights are updated according to the following rules.

$$\begin{aligned}\frac{d\theta_y}{dt} &= \sum_{t=0}^T \epsilon_{y_t} \frac{dg(\theta_y h_t)}{d\theta_y} h_t^T \\ \frac{d\theta_x}{dt} &= \sum_{t=0}^T \epsilon_{h_t} \frac{df(\theta_h h_{t-1} + \theta_x x_t)}{d\theta_x} x_t^T \\ \frac{d\theta_h}{dt} &= \sum_{t=0}^T \epsilon_{h_t} \frac{df(\theta_h h_{t-1} + \theta_x x_t)}{d\theta_h} h_{t+1}^T\end{aligned}$$

Since the RNN feedforward updates are parameter-linear, these rules are Hebbian, only requiring the multiplication of pre and post-synaptic potentials. This means that the predictive coding updates proposed here are biologically plausible and could in theory be implemented in the brain. The only biological implausibility remains the BPTT learning scheme.

Our RNN was trained on a simple character-level name-origin dataset which can be found here: <https://download.pytorch.org/tutorial/data.zip>. The RNN was presented with sequences of characters representing names and had to predict the national origin of the name – French, Spanish, Russian, etc. The characters were presented to the network as one-hot-encoded vectors without any embedding. The output categories were also presented as a one-hot vector. The RNN has a hidden size of 256 units. A *tanh* nonlinearity was used between hidden states and the output layer was linear. The network was trained on randomly selected name-category pairs from the dataset. The training loss for the predictive coding and backprop RNNs, averaged over 5 seeds is presented below (Figure 7).

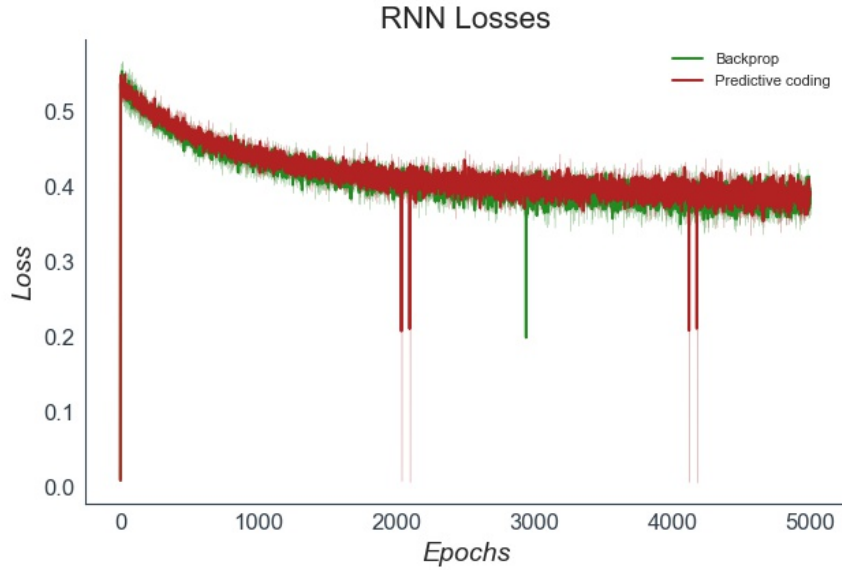


Figure 7: Training losses for the predictive coding and backprop RNN. As expected, they are effectively identical.

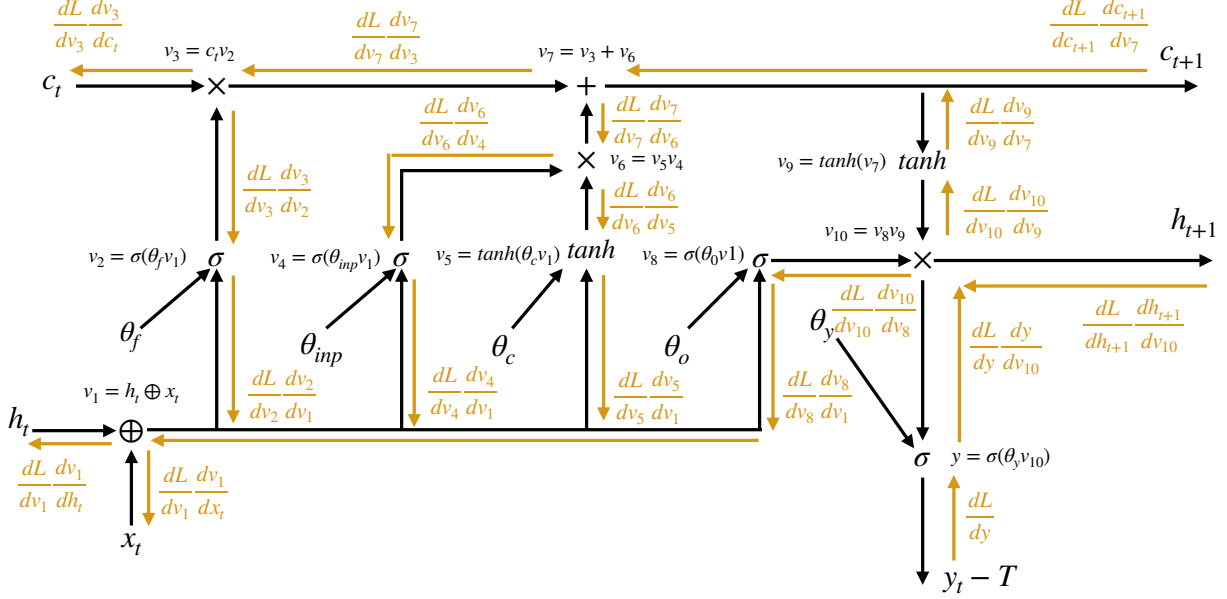


Figure 8: Computation graph and backprop learning rules for a single LSTM cell.

Appendix D: Predictive Coding LSTM Implementation Details

Unlike the other two models, the LSTM possesses a complex and branching internal computation graph, and is thus a good opportunity to make explicit the predictive coding ‘recipe’ for approximating backprop on arbitrary computation graphs. The computation graph for a single LSTM cell is shown (with backprop updates) in Figure 8. Prediction for the LSTM occurs by simply rolling forward a copy of the LSTM cell for each timestep. The LSTM cell receives its hidden state h_t and cell state c_t from the previous timestep. During training we compute derivatives on the unrolled computation graph and receive backwards derivatives (or prediction errors) from the LSTM cell at time $t + 1$.

The equations that specify the computation graph of the LSTM cell are as follows.

$$\begin{aligned}
 v_1 &= h_t \oplus x_t \\
 v_2 &= \sigma(\theta_i v_1) \\
 v_3 &= c_t v_2 \\
 v_4 &= \sigma(\theta_{inp} v_1) \\
 v_5 &= \tanh(\theta_c v_1) \\
 v_6 &= v_4 v_5 \\
 v_7 &= v_3 + v_6 \\
 v_8 &= \sigma(\theta_o v_1) \\
 v_9 &= \tanh(v_7) \\
 v_{10} &= v_8 v_9 \\
 y &= \sigma(\theta_y v_{10})
 \end{aligned}$$

The recipe to convert this computation graph into a predictive coding algorithm is straightforward. We first rewrite the connectivity so that the predictions are set to the forward functions of their parents. We then compute the errors

between the vertices and the predictions.

$$\begin{aligned}
\mu_1 &= h_t \oplus x_t \\
\mu_2 &= \sigma(\theta_i v_1) \\
\mu_3 &= c_t v_2 \\
\mu_4 &= \sigma(\theta_{inp} v_1) \\
\mu_5 &= \tanh(\theta_c v_1) \\
\mu_6 &= v_4 v_5 \\
\mu_7 &= v_3 + v_6 \\
\mu &= \sigma(\theta_o v_1) \\
\mu_9 &= \tanh(v_7) \\
\mu_{10} &= v_8 v_9 \\
\mu_y &= \sigma(\theta_y v_{10}) \\
\epsilon_1 &= v_1 - \mu_1 \\
\epsilon_2 &= v_2 - \mu_2 \\
\epsilon_3 &= v_3 - \mu_3 \\
\epsilon_4 &= v_4 - \mu_4 \\
\epsilon_5 &= v_5 - \mu_5 \\
\epsilon_6 &= v_6 - \mu_6 \\
\epsilon_7 &= v_7 - \mu_7 \\
\epsilon_8 &= v_8 - \mu_8 \\
\epsilon_9 &= v_9 - \mu_9 \\
\epsilon_{10} &= v_{10} - \mu_{10}
\end{aligned}$$

During inference, the inputs h_t, x_t and the output y_t are fixed. The vertices and then the prediction errors are updated according to Equation 1. This recipe is straightforward and can easily be extended to other more complex machine learning architectures. The full augmented computation graph, including the vertex update rules, is presented in Figure 9.

Empirically, we observed rapid convergence to the exact backprop gradients even in the case of very deep computation graphs (as is an unrolled LSTM with a sequence length of 100). Although convergence was slower than was the case for CNNs or lesser sequence lengths, it was still straightforward to achieve convergence to the exact numerical gradients with sufficient iterations.

Below we plot the mean divergence between the predictive coding and true numerical gradients as a function of sequence length (and hence depth of graph) for a fixed computational budget of 200 iterations with an inference learning rate of 0.05. As can be seen, the divergence increases roughly linearly with sequence length. Importantly, even with long sequences, the divergence is not especially large, and can be decreased further by increasing the computational budget. As the increase is linear, we believe that predictive coding approaches should be scalable even for backpropagating through very deep and complex graphs.

Our architecture consisted of a single LSTM layer (more complex architectures would consist of multiple stacked LSTM layers). The LSTM was trained on a next-character character-level prediction task. The dataset was the full works of Shakespeare, downloadable from Tensorflow. The text was shuffled and split into sequences of 50 characters, which were fed to the LSTM one character at a time. The LSTM was trained then to predict the next character, so as to ultimately be able to generate text. The characters were presented as one-hot-encoded vectors. The LSTM had a

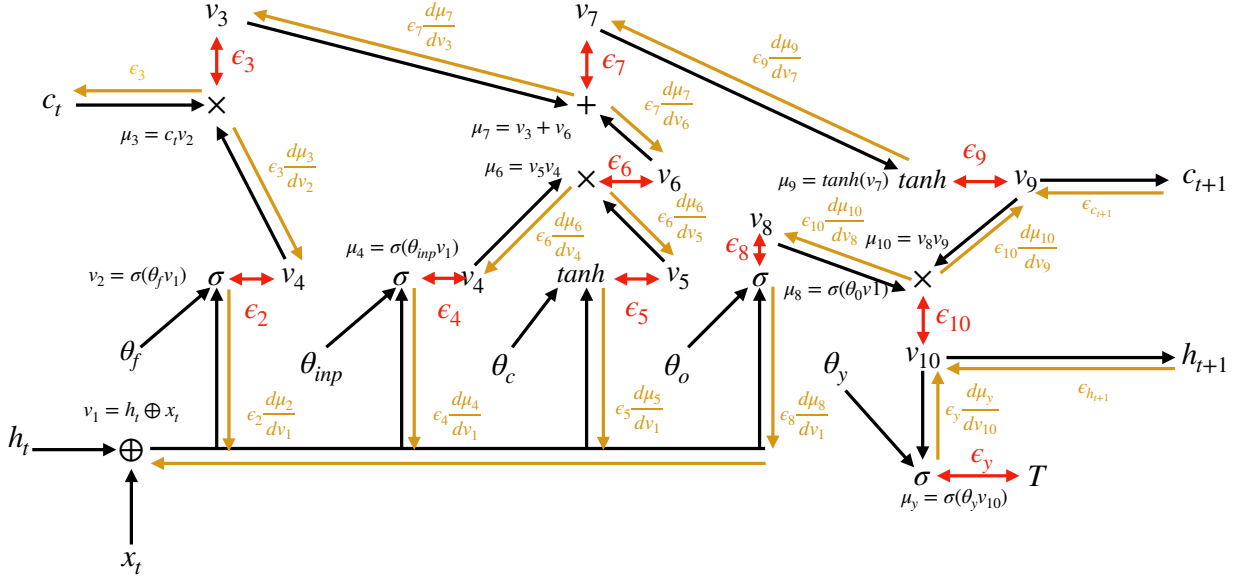


Figure 9: The LSTM cell computation graph augmented with error units, evincing the connectivity scheme of the predictive coding algorithm.

hidden size and a cell-size of 1056 units. A minibatch size of 64 was used and a weight learning rate of 0.0001 was used for both predictive coding and backprop networks. To achieve sufficient numerical convergence to the correct gradient, we used 200 variational iterations with an inference learning rate of 0.1. This rendered the predictive LSTM approximately 200x as costly as the backprop LSTM to run. A graph of the LSTM training loss for both predictive coding and backprop LSTMs, averaged over 5 random seeds, can be found below (Figure 11).

Appendix E: Properties of the Inner-Optimization

The inner optimization loop of the predictive coding algorithm, where the vs are iterated until reaching a fixed point is the source of the significant computational overhead compared to backprop. Since each iteration in the inner loop has a computational cost roughly proportional to a backwards backpropagation pass, our method is approximately N times slower than backprop where N is the number of variational iterations required to reach convergence. We typically find that 50-200 iterations is sufficient to achieve very good numerical convergence to the analytical gradients with deeper computation graphs requiring slightly more iterations to converge.. This number of iterations is both small and large. It is small compared to total number of iterations typically needed to train the network as a whole using backprop, thus testifying to the relative 'niceness' of the underlying optimization problem, however it is also large in that it incurs a significant computational cost. Since neural networks using backprop are already running up against limits of computational capacity, this additional overhead means that predictive coding implementations will always lag behind the performance of the machine learning state of the art due to this overhead. It is important to note additionally that this computational cost is primarily an issue due to the serial computational nature of electronic computers. In the brain, the convergence of the network may not be as expensive since it can be done in parallel across the brain as a dynamic relaxation. Similarly, this iteration algorithm could also perhaps be performed in an extremely efficient way by analog circuitry.

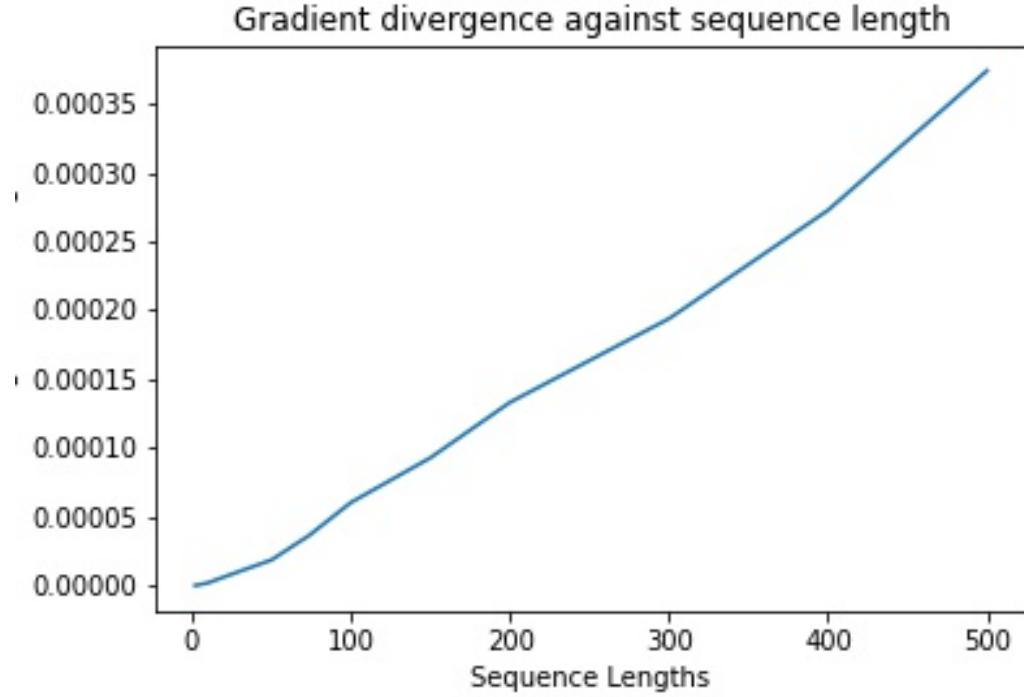


Figure 10: Divergence between predictive coding and numerical gradients as a function of sequence length.

Nevertheless, there remains an issue with the inner optimisation, which applies to its implementation in neural circuitry is simply the time it takes to do. The brain is not presented with individual stimuli and then given however long it needs to prepare a response. Instead it must navigate a dynamic world with constantly shifting inputs, some requiring extremely fast responses. Fifty forward-backward iterations through the brain would take much too long to be able to adequately respond to many important, survival-relevant stimuli, thus rendering a direct or naive implementation of this predictive coding algorithm in the brain unlikely. However, there are two possible solutions. Firstly, it is possible that the inner-optimisation problem is fundamentally convex, as discussed below, and thus there may be substantially more efficient means of solving it than a naive gradient descent. Secondly, the brain is not presented with individual i.i.d stimuli presented at random from some dataset, but rather with a dynamically and largely slowly changing world where what is presented at time $t + 1$ has substantial correlations with what was seen at time t . Due to these correlations in the input, internal brain states may effectively always be 'surfing' near the optimum value already, and so need only change a relatively small amount upon the presentation of new stimuli.

Empirically, we have found that unlike the overall optimisation problem of the weights, the optimisation problem for the vs is very "nice" and, if not completely convex, has many desirable properties. In general we found that convergence is very quick (within 200 iterations) even for very deep computation graphs such as an unrolled LSTM over hundreds of items in a sequence (Figure 10). Moreover, the optimisation is very stable and allows the use of very high learning rates (such as 0.1) which would cause divergence if used on the weights. Finally, and this is a crucial point, there do not appear to be issues with local minima, as in all our experiments the inner optimisation converged directly to the analytically correct gradients (within a small tolerance which can be reduced with further iteration). Never did we observe the inner optimisation attain a local minima – i.e. incorrect gradients. This leads us to hypothesise that the inner optimisation has only a single global minimum, and may be convex, even in the case of deep and nonlinear computation graphs. This seems to be a surprising hypothesis given that the underlying computation graph can be made extremely

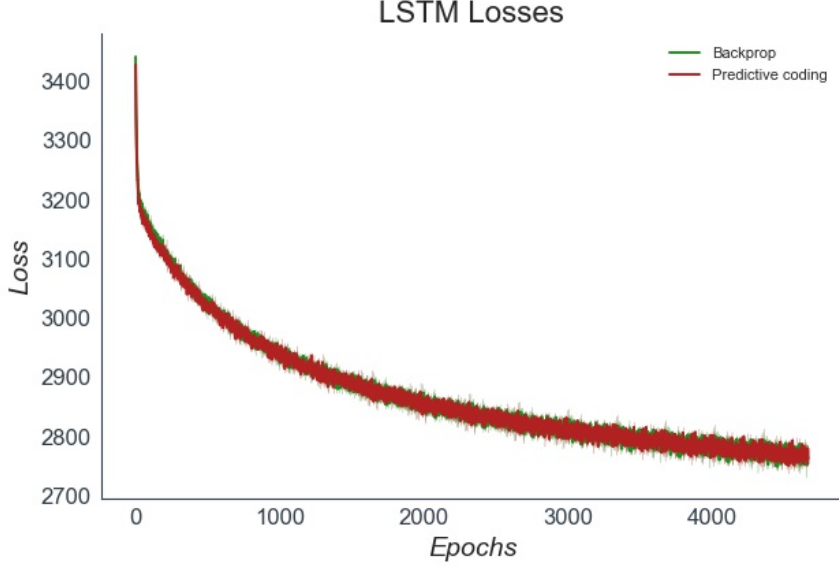


Figure 11: Training losses for the predictive coding and backprop LSTMs averaged over 5 seeds. The performance of the two training methods is effectively equivalent.

complex and nonlinear, and we can offer no proof of this in the general nonlinear case, although we have shown some tantalising empirical results. We present a proof of convexity in the linear regime below.

If the inner optimisation problem were convex, or approximately so, in the general nonlinear case, this would be of great utility for the scalability of predictive coding algorithms, since it would enable the use of powerful convex optimisation algorithms (Boyd, Boyd, & Vandenberghe, 2004) which could find the equilibrium of the v 's much more efficiently than the naive gradient descent methods we use here. Since the inner optimisation is the primary source of computational overhead compared to backprop, then this could substantially increase the scalability of our method, to perhaps be somewhat competitive with backprop and would enable the training of significantly more complex predictive coding architectures from the machine learning literature

Convexity in the Linear Regime

Here we show that the inner optimization process is convex in the linear regime. The key quantity to compute is the Hessian of the free energy with respect to the activations. If the Hessian is positive definite everywhere the function is convex.

We have defined the free-energy $F = \sum_i \epsilon_i^2$ as the sum of prediction errors between the activations v_i at a 'layer' and the predictions μ_i from the layer below.

$$\epsilon_i = v_i - \mu_i$$

where $\mu_i = f(v_{i-1})$. For the global function to be convex we require that the Hessian $\frac{d^2 F}{dv_i^2}$ to be convex for all v_i . In general since the overall free-energy is simply the sum as the layer-wise free-energies, it suffices to consider a single

$\frac{d^2 F}{dv_i^2}$. We can calculate:

$$\begin{aligned}
 \frac{d^2 F}{dv_i^2} &= \frac{d^2 \epsilon_i^2}{dv_i^2} + \frac{d^2 \epsilon_{i+1}^2}{dv_i^2} \\
 &= \mathbf{I} + \frac{d}{dv_i} [\epsilon_{i+1} \frac{d\mu_{i+1}}{dv_i}] \\
 &= \underbrace{\mathbf{I}}_{\text{Positive Definite}} + \underbrace{\epsilon_{i+1} \frac{d^2 \mu_{i+1}}{dv_i^2}}_{\text{Unknown}} + \underbrace{\frac{d\mu_{i+1}}{dv_i}^T \frac{d\mu_{i+1}}{dv_i}}_{\text{Positive Definite}}
 \end{aligned} \tag{6}$$

For the problem to be convex we require that:

$$\mathbf{I} + \frac{d\mu_{i+1}}{dv_i}^T \frac{d\mu_{i+1}}{dv_i} \geq -\epsilon_{i+1} \frac{d^2 \mu_{i+1}}{dv_i^2} \tag{7}$$

Which is not obviously true in the general case. The key difficulty is proving that the $\epsilon_{i+1} \frac{d^2 \mu_{i+1}}{dv_i^2}$ term is positive definite either in all situations.

In the linear case convexity is guaranteed since when the predictions are linear we have $\mu_{i+1} = \theta_i y_i$ and thus $\frac{d^2 \mu_{i+1}}{dv_i^2} = 0$. This means that the middle term drops out and we are left with:

$$\frac{d^2 F}{dv_i^2} = \mathbf{I} + \theta_i^T \theta_i \tag{8}$$

Which is always positive definite and therefore the inner optimization is convex in the linear regime.

Appendix F: Derivation of the Free Energy Functional

Here we derive in detail the form of the free-energy functional used in sections 2 and 4. We also expand upon the assumptions required and the precise form of the generative model and variational density. Much of this material is presented with considerably more detail in Buckley et al. (2017), and more approachably in Bogacz (2017).

Given an arbitrary computation graph with vertices $y_{0:N-1}$ (note - not v_i), we treat these vertices as random variables who's value is to be inferred. Given an input y_0 and a target y_N (the multiple input and/or output case is a straightforward generalization). We wish to infer the posterior $p(y_{1:N-1}|y_0, y_N)$. We approximate this intractable posterior with variational inference. Variational inference proceeds by defining an approximate posterior $Q(y_{1:N-1}; \phi)$ with some arbitrary parameters ϕ . We then wish to minimize the KL divergence between the true and approximate posterior.

$$\operatorname{argmin}_{\phi} \mathbb{KL}[Q(y_{1:N-1}; \phi) \| p(y_{1:N-1}|y_0, y_N)]$$

Although this KL is itself intractable, since it includes the intractable posterior, we can derive a tractable bound on this KL called the variational free-energy.

$$\begin{aligned}
 \mathbb{KL}[Q(y_{1:N-1}; \phi) \| p(y_{1:N-1}|y_0, y_N)] &= \mathbb{KL}[Q(y_{1:N-1}) \| \frac{p(y_{1:N-1}, y_0, y_N)}{p(y_0, y_N)}] \\
 &= \mathbb{KL}[Q(y_{1:N-1}; \phi) \| p(y_{1:N-1}, y_0, y_N)] + \ln p(y_0, y_N) \\
 \Rightarrow \underbrace{\mathbb{KL}[Q(y_{1:N-1}; \phi) \| p(y_{1:N-1}, y_0, y_N)]}_{-\mathcal{F}} &\leq \mathbb{KL}[Q(y_{1:N-1}; \phi) \| p(y_{1:N-1}|y_0, y_N)]
 \end{aligned} \tag{9}$$

We define the negative free-energy $-\mathcal{F} = \mathbb{KL}[Q(y_{1:N-1}) \| p(y_{1:N-1}, y_0, y_N)]$ which is a lower bound on the divergence between the true and approximate posteriors. By thus maximizing the negative free-energy (which is identical to the ELBO (Beal et al., 2003; Blei, Kucukelbir, & McAuliffe, 2017), or equivalently minimizing the free-energy, we decrease this divergence and make the variational distribution a better approximation to the true posterior.

To proceed further, it is necessary to define an explicit form of the generative model $p(y_0, y_{1:N-1}, y_N)$ and the approximate posterior $Q(y_{1:N-1}; \phi)$. In predictive coding, we define a hierarchical Gaussian generative model which mirrors the exact structure of the computation graph

$$p(y_{0:N}) = \mathcal{N}(y_0; \bar{y}_0, \Sigma_0) \prod_{i=1}^N \mathcal{N}(y_i; f(\text{Par}(y_i); \theta_{y_j \in \text{Par}(y_i)}), \Sigma_i);$$

Where essentially each vertex y_i is a Gaussian with a mean which is a function of the prediction of all the parents of the vertex, and the parameters of their edge-functions. \bar{y}_0 is effectively an "input-prior" which is set to 0 throughout and ignored. The output vertices $y_N = T$ are set to the target T .

We also define the variational density to be Gaussian with mean $v_{1:N-1}$ and variance $\sigma_{1:N-1}$, but under a mean field approximation, so that the approximation at each node is independent of all others (note the variational variance is denoted σ while the variance of the generative model is denoted Σ . The lower-case σ is not used to denote a scalar variable – both variances can be multivariate – but to distinguish between variational and generative variances)

$$Q(y_{1:N-1}; v_{1:N-1}, \sigma_{1:N-1}) = \prod_{i=1}^{N-1} \mathcal{N}(y_i; v_i, \sigma_i)$$

We now can express the free-energy functional concretely. First we decompose it as the sum of an energy and an entropy

$$\begin{aligned} -\mathcal{F} &= \mathbb{KL}[Q(y_{1:N-1}; v_{1:N-1}, \sigma_{1:N-1}) \| p(y_0, y_{1:N-1}, y_N)] \\ &= \underbrace{-\mathbb{E}_{Q(y_{1:N-1}; v_{1:N-1}, \sigma_{1:N-1})}[\ln p(y_0, y_{1:N-1}, y_N)]}_{\text{Energy}} + \underbrace{\mathbb{E}_{Q(y_{1:N-1}; v_{1:N-1}, \sigma_{1:N-1})}[\ln Q(y_{1:N-1}; v_{1:N-1}, \sigma_{1:N-1})]}_{\text{Entropy}} \end{aligned}$$

Then, taking the entropy term first, we can express it concretely in terms of normal distributions.

$$\begin{aligned} \mathbb{E}_{Q(y_{1:N-1}; v_{1:N-1}, \sigma_{1:N-1})}[\ln Q(y_{1:N-1}; v_{1:N-1}, \sigma_{1:N-1})] &= \mathbb{E}_{Q(y_{1:N-1}; v_{1:N-1}, \sigma_{1:N-1})}[\sum_{i=1}^{N-1} \ln \mathcal{N}(y_i; v_i, \sigma_i)] \\ &= \sum_{i=1}^{N-1} \mathbb{E}_{Q(y_i; v_i, \sigma_i)}[\ln \mathcal{N}(y_i; v_i, \sigma_i)] \\ &= \sum_{i=1}^{N-1} \mathbb{E}_{Q(y_i; v_i, \sigma_i)}[-\frac{1}{2} \ln \det(2\pi\sigma_i)] + \mathbb{E}_{Q(y_i; v_i, \sigma_i)}[\frac{(y_i - v_i)^2}{2\sigma_i}] \\ &= \sum_{i=1}^{N-1} -\frac{1}{2} \ln \det(2\pi\sigma_i) + \frac{\sigma_i}{2\sigma_i} \\ &= \frac{N}{2} + \sum_{i=1}^{N-1} -\frac{1}{2} \ln \det(2\pi\sigma_i) \end{aligned}$$

The entropy of a multivariate gaussian has a simple analytical form depending only on the variance. Next we turn to the energy term, which is more complex. To derive a clean analytical result, we must make a further assumption, the Laplace approximation which requires the variational density to be tightly peaked around the mean so the only non-negligible contribution to the expectation is from regions around the mean. This means that we can successfully approximate the approximate posterior with a second-order Taylor expansion around the mean. From the first line

onwards we ignore the $\ln p(y_0)$ and $\ln p(y_N|\text{Par}(y_N))$ which lie outside the expectation.

$$\begin{aligned}
\mathbb{E}_{Q(y_{1:N-1}; v_{1:N-1}, \sigma_{1:N-1})}[\ln p(y_{0:N})] &= \ln p(y_0) + \ln p(y_N|\text{Par}(y_N)) + \sum_{i=1}^{N-1} \mathbb{E}_{Q(y_i; v_i, \sigma_i)}[\ln p(y_i|\text{Par}(y_i))] \\
&= \sum_{i=1}^N E_Q[\ln p(v_i|\text{Par}(y_i))] + E_Q\left[\frac{d \ln p(y_i|\text{Par}(y_i))}{dy_i}(v_i - y_i)\right] \\
&\quad + E_Q\left[\frac{d^2 \ln p(v_i|\text{Par}(y_i))}{dy_i^2}(v_i - y_i)^2\right] \\
&= \sum_{i=1}^N \ln p(v_i|\text{Par}(y_i)) + \frac{d^2 \ln p(v_i|\text{Par}(y_i))}{dy_i^2} \sigma_i
\end{aligned}$$

Where the second term in the Taylor expansion evaluates to 0 since $E_Q[y_i - v_i] = (v_i - v_i) = 0$ and the third term contains the expression for the variance $E_Q[(y_i - v_i)^2] = \sigma_i$.

We can then write out the full Laplace-encoded free-energy as:

$$-\mathcal{F} = \sum_{i=1}^N \ln p(v_i|\text{Par}(y_i)) + \frac{d^2 \ln p(v_i|\text{Par}(y_i))}{dy_i^2} \sigma_i - \frac{1}{2} \ln \det(2\pi\sigma_i)$$

We wish to minimize \mathcal{F} with respect to the variational parameters v_i and σ_i . There is in fact a closed-form expression for the optimal variational variance which can be obtained simply by differentiating and setting the derivative to 0.

$$\begin{aligned}
\frac{d\mathcal{F}}{d\sigma_i} &= \frac{d^2 \ln p(v_i|\text{Par}(y_i))}{dy_i^2} - \sigma_i^{-1} \\
\frac{d\mathcal{F}}{d\sigma_i} = 0 \Rightarrow \sigma_i^* &= \frac{d^2 \ln p(v_i|\text{Par}(y_i))}{dy_i^2}^{-1}
\end{aligned}$$

Because of this analytical result for the variational variance, we do not need to consider it further in the optimisation problem, and only consider minimizing the variational means v_i . This renders all the terms in the free-energy except the $\ln p(v_i|\text{Par}(y_i))$ terms constant with respect to the variational parameters. This allows us to write:

$$-\mathcal{F} \approx \ln p(y_N|\text{Par}(y_N)) + \sum_{i=1}^N \ln p(v_i|\text{Par}(y_i)) \quad (10)$$

as presented in section 2. The first term $\ln p(y_N|\text{Par}(y_N))$ is effectively the loss at the output ($y_N = T$) so becomes an additional prediction error $\ln p(y_N|\text{Par}(y_N)) \propto (T - \mu_N)^T \Sigma_N^{-1} (T - \mu_N)$ which can be absorbed into the sum over other prediction errors. Crucially, although the variational variances have an analytical form, the variances of the generative model (the precisions Σ_i) do not and can be optimised directly to improve the log model-evidence. These precisions allow for a kind of 'uncertainty-aware' backprop.

Derivation of Variational Update Rules and Fixed points

Here, starting from Equation 10, we show how to obtain the variational update rule for the v_i 's (Equation 1), and the fixed point equations (Equation 2) (Bogacz, 2017; Friston, 2005, 2008). We first reduce the free-energy to a sum of prediction errors.

$$\begin{aligned}
-\mathcal{F} &\approx \sum_{i=1}^N \ln p(v_i|\text{Par}(v_i)) \\
&\approx \sum_{i=1}^N (v_i - f(\text{Par}(v_i)))^T \Sigma_i^{-1} (v_i - f(\text{Par}(v_i)))^T + \ln 2\pi \Sigma_i^{-1} \\
&= \sum_{i=1}^N \epsilon_i^T \epsilon_i + \ln 2\pi \text{Sigma}_i^{-1}
\end{aligned}$$

Where $\epsilon_i = v_i - f(\text{Par}(v_1))$, and we have utilized the assumption made in section 2 that $\Sigma^{-1} = \mathbf{I}$. By setting all precisions to the identity, we are implicitly assuming that all datapoints and vertices of the computational graph have equal variance. Next we assume that the dynamics of each vertex v_i follow a gradient descent on the free-energy.

$$\begin{aligned} -\frac{dv_i}{dt} &= \frac{d\mathcal{F}}{dv_i} = \frac{d}{dv_i} \left[\sum_{j=1}^N \epsilon_j^T \epsilon_j \right] \\ &= \epsilon_i \frac{d\epsilon_i}{dv_i} + \sum_{j \in \text{Chi}(v_i)} \epsilon_j \frac{d\epsilon_j}{dv_i} \\ &= \epsilon_i - \sum_{j \in \text{Chi}(v_i)} \epsilon_j \frac{d\mu_j}{dv_i} \end{aligned}$$

Where we have used the fact that $\frac{d\epsilon_i}{dv_i} = 1$ and $\frac{d\epsilon_j}{dv_j} = -\frac{d\mu_j}{dv_i}$. To obtain the fixed point of the dynamics, we simply solve for $\frac{dv_i}{dt} = 0$.

$$\begin{aligned} \frac{dv_i}{dt} &= \frac{d\mathcal{F}}{dv_i} = 0 \\ \Rightarrow 0 &= \epsilon_i - \sum_{j \in \text{Chi}(v_i)} \epsilon_j \frac{d\mu_j}{dv_i} \\ \Rightarrow \epsilon_i^* &= \sum_{j \in \text{Chi}(v_i)} \epsilon_j \frac{d\mu_j^*}{dv_i^*} \end{aligned}$$

Similarly, since $\epsilon_i^* = v_i^* - \mu_i^*$ then $v_i^* = \epsilon_i^* + \mu_i^*$. So:

$$\begin{aligned} v_i^* &= \epsilon_i^* + \mu_i^* \\ &= \mu_i^* - \sum_{j \in \text{Chi}(v_i)} \epsilon_j \frac{d\mu_j^*}{dv_i^*} \end{aligned}$$